

Sodium-coupled Secondary Transporters

11

Insights from Structure-based Computations

Elia Zomot, Ahmet Bakan, Indira H. Shrivastava, Jason DeChancie,
Timothy R. Lezon and Ivet Bahar

1. Introduction: Biological Function and Classification

The biological membrane bilayer is impermeable to almost all polar or charged molecules. In order for the various solutes to cross this barrier, integral membrane proteins have evolved to provide a hydrophilic environment within the membrane that can bind and translocate these solutes into or out of the cell, often against their electrochemical gradient. These transporters are conventionally classified into three classes on the basis of the energy source used for transport: (1) primary active transporters rely on light, hydrolysis of ATP or redox reactions, (2) secondary active transporters require the electrochemical gradient of ions across the membrane to power the “uphill” translocation of the substrate, and (3) precursor/product antiporters exchange one molecule with its metabolic product independent of another source of energy.^{1,2}

A major family of secondary transporters involves sodium- (and less often proton-) dependent symporters that couple the energy-costly translocation of the solute into the cell to that of sodium down its electrochemical gradient. These sodium-coupled transporters are found in all species and participate in a myriad biological functions, e.g. maintenance of efficient neurotransmission,^{3,4,5} absorption of nutrients in the intestine,⁶ regulation of pH and cytoplasmic $[\text{Na}^+]^{7,8}$ and osmoregulation^{9,10} are only some of their physiological functions.

Of particular interest among sodium-coupled symporters are two families: the dicarboxylate/amino-acid:cation symporters (DAACS) and the neurotransmitter sodium symporters (NSS). The DAACS and NSS keep the extracellular (EC) neurotransmitter concentrations sufficiently low at the synaptic cleft, which enables postsynaptic receptors to detect signaling by the presynaptic nerve cell in the form of exocytotically released transmitters (Figure 1). The DAACS and NSS are key elements in the termination of the synaptic action of neurotransmitters, which is accomplished by diffusion and re-uptake of neurotransmitters into neuronal or glial cells; the single exception in this regard involves acetylcholine-mediated signal transmission.

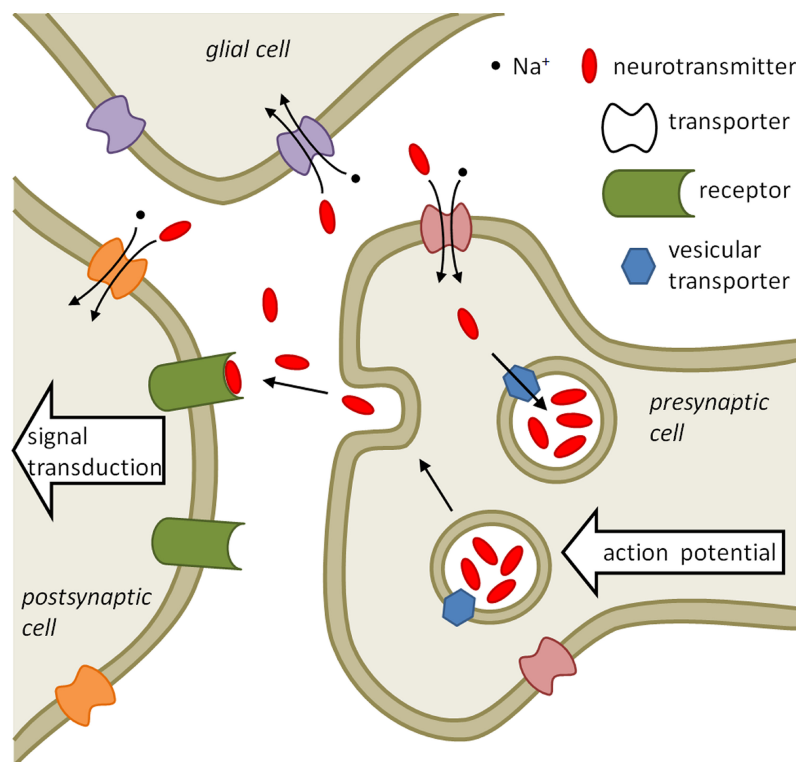


Figure 1. Simplified depiction of the role of neurotransmitter transporters. An arriving action potential in the presynaptic cell causes the fusion of neurotransmitter-loaded vesicles with the cell membrane and the release of their content into the synaptic cleft. Therein, the released neurotransmitter binds receptors on the postsynaptic cell membrane initiating a signal transduction pathway by inducing an action potential and/or a metabolic cascade. In order to induce a subsequent postsynaptic signal, the neurotransmitter has to be cleared from the synaptic cleft and this function is carried out by neurotransmitter transporters which couple the intake of the neurotransmitter to the transport of sodium ions into the pre-synaptic, postsynaptic or glial cells. The vesicular transporters — which are proton-dependent — load the pre-synaptic vesicles with neurotransmitter from the cytoplasm.

The DAACS family includes the glutamate (Glu^-) transporters (GluTs), also called excitatory amino acid transporters (EAATs) in humans. GluTs are located on neurons and glia (astrocytes) where they clear the excess Glu^- released at the synapses (Figure 1). The concentration of Glu^- in the EC space may increase by 10^3 – 10^4 fold during periods of synaptic activation. Accumulation of Glu^- above physiological (mM) levels may cause neurotoxic effects. Glu^- uptake and re-uptake by GluTs is essential for controlling EC levels of Glu^- ,^{11,12} thereby regulating glutamatergic signal transmission, i.e. preventing sustained activation and desensitization of ionotropic receptors, modulating the activation of metabotropic receptors,¹³ and assisting in the glutamate-glutamine cycle.¹⁴ The transport of Glu^- by GluTs is facilitated by the sodium electrochemical gradient.^{15,16,17} The aspartate (Asp^-) transporter from *Pyrococcus horikoshii*, Glt_{ph} , is the only member of this family that has been structurally resolved to date,^{18,19,20} and has significantly assisted in improving our understanding of the potential molecular mechanisms that control the activity of GluTs.

The NSS family members, on the other hand, translocate small molecules that may be neurotransmitters, such as γ -aminobutyric acid (GABA), dopamine, serotonin or norepinephrine, or even amino acids such as leucine or tyrosine. The leucine transporter from *Aquifex aeolicus* (LeuT), later found to be a more efficient transporter of alanine, has served as a structural paradigm for this family after the resolution of its structure with bound substrate and sodium ions.²¹

Since transporter function is to regulate neurotransmitter activity by removing the transmitters from the synaptic cleft, specific transporter inhibitors (or enhancers/agonists) can potentially be used as novel drugs for neurological diseases. Inhibitors that block the biogenic amine transporters include antidepressant drugs (e.g. Prozac) and stimulants (e.g. amphetamines and cocaine).^{22,23} GluTs, in particular GLT-1, play a central role in preventing both hyperexcitability and excitotoxicity,¹¹ which are implicated in epilepsy, stroke and Huntington's disease. Therefore, Na⁺-coupled neurotransmitter transporters are of considerable medical interest.

Notably, many Na⁺-coupled transporters belonging to other families have been found — upon resolution of their crystal structure — to share the LeuT structural fold despite their lack of significant sequence similarity, inviting attention to the functional versatility of this particular fold for transporting solutes across the membrane (Table 1). These include the galactose transporter from *Vibrio parahaemolyticus* (vSGLT) of the sodium solute symporters (SSS) family, the benzylhydantoin transporter (Mhp1) of the nucleobase cation symporters (NCS1) family, and the betaine transporter (BetP) of the betaine/choline/carnitine transporters (BCCT) family. Of these, the SSS family members transport sugars, inorganic ions, vitamins and choline.²⁴ SGLT1-6, for instance, are found in various tissues, such as the heart, kidney and intestine, and are responsible for the transport and absorption of glucose, galactose and mannose.^{24,25} Genetic disorders of SGLTs include glucose-galactose malabsorption and familial renal glucosuria.^{25,26,27} SGLT1 plays a central role in oral rehydration therapy to treat secretory diarrhea (e.g. cholera) and increased attention is being focused on SGLTs as drug targets for diabetic therapy.

In addition, the LeuT fold has been recently found to be shared by transporters that are not sodium-coupled. These are the arginine/arginine antiporter (AdiC) of the APC family and the carnitine/ γ -butyrobetaine antiporter (CaiT) of the BCCT family. It is worth noting that whereas prokaryotic and eukaryotic members of the NSS family share about 20–25% sequence identity, there is practically no sequence similarity between LeuT and the above listed structurally similar members of the SSS, NCS1 or BCCT families. As to GluTs, the five isoforms, EAAT1-5, share 50–60% sequence identity among themselves, and exhibit about 20–30% sequence identity with the bacterial transporters in the DAACS family, but share no significant homology with the NSS family members.

A full summary of the sodium-coupled secondary transporters with resolved structures (along with the transporters that have the same fold but are not sodium-coupled) is presented in Table 1. We note that in addition to the LeuT and Glt_{ph} folds, a third fold of a representative member (NhaA) of the Na⁺/H⁺ antiporter family has been recently identified. In the present chapter, we focus on the functional dynamics of the DAACS and NSS families, using the respective Glt_{ph} and LeuT folds as structural prototypes. Section 2 provides a macroscopic description of their Na⁺-coupled mechanism, based on thermodynamics arguments. Sections 3 and 4 summarize our current understanding of their substrate translocation mechanisms at the microscopic/molecular level, based on the resolved structures and on recent structure-based computations.

Table 1. Properties of Na⁺-coupled transporters and their structural homologs resolved to date by X-ray crystallography.

Fold	LeuT						GltPh	NhaA		
	Transporter	LeuT	Mhp1	vSGLT	BetP	CaiT			AdiC1	ApcT
Family	Neurotransmitter/Sodium Symporters (NSS)	Neurotransmitter/Sodium Symporters (NSS)	Nucleobase/Cation Symporters (NCS1)	Sodium/Solute Symporters (SSS)	Betaine/Choline/Carnitine Transporters (BCCT)	Amino Acid/Polyamine/Organocation Transporters (APC)	Dicarboxylic Amino-Acid: Cation Symporters (DAACS)	Sodium/Proton Antiporters		
Oligomeric state	Dimer	Dimer	Dimer	Dimer	Trimer	Dimer	Trimer	Dimer		
Repeating helices	'1-5' + '6-10'	'1-5' + '6-10'	'1-5' + '6-10'	'2-6' + '7-11'	'3-7' + '8-12'	'1-5' + '6-10'	'1-3, 7, HP1' + '4-6, 8, HP2'	'3-5' + '10-12'		
Crystallized conformation	1) Outward-facing occluded 2) Outward-facing open 3) Inward-facing open	1) Outward-facing occluded 2) Outward-facing open 3) Inward-facing open	Inward-facing occluded*	Inward-facing Intermediate-occluded	Inward-facing	1) Outward-facing occluded 2) Outward-facing open	1) Outward-facing open 2) Outward-facing-occluded 3) Inward-facing occluded	Inward-facing		
Substrate(s)**	Leucine, glycine, alanine,... + Na ⁺	Benzylhydantoin + Na ⁺	Galactose + Na ⁺	Glycine-betaine + Na ⁺	Carnitine/ γ -butyrobetaine	Arginine/ agmatine	Alanine, glycine, glutamine,... + H ⁺	Aspartate + Na ⁺	2H ⁺ /Na ⁺	
PDB accession code	2A65, 3F4G, 3F3A, 3F4J, 2Q6H, 2QE1	2JLN, 2JLO, 2X79	3DH4	2WIT	3HFX	3LRC, 3LIL, 3GIA	1XFH, 2NWL, 2NWW, 2NWX, 3KBC	1ZCD		

* Only the galactose, but not the sodium ion, is occluded from the IC in this conformation.^{28,29,30}** "+ Na⁺" indicates co-transport with one or more Na⁺ ions whereas "n" indicates antiport.

2. Na⁺-Coupled Mechanism of Transport: A Macroscopic View

2.1 Transport cycle and alternating access mechanism

In order for transporters to carry out their function, the substrate needs to be alternately exposed to either side of the membrane: the binding of the substrate and co-transported ions takes place on one side, and their release, on the other. The notion that a transporter can exist in either an outward- or an inward-facing state has been subject to debate for decades.³¹ Recently obtained crystal structures of several transporters clearly demonstrate the occurrence of an outward- or inward-facing state consistent with the alternating access mechanism.^{19,20,32–34}

A typical transport cycle for a Na⁺-coupled symporter is initiated by binding the substrate and co-transported sodium ions (or protons) from the EC medium. For this to occur, the transporter has to be in a conformation where the external aqueous cavity provides access to the binding site (Figure 2a). Following binding, the external cavity may remain open, but the substrate may be shielded from the external medium by one or more hydrophobic side-chains of the protein, as in the cases of LeuT and BetP,^{10,21} or by a small loop as in Glt_{ph}. Such a state is often referred to as the outward-facing occluded form (Figure 2b). The transporter then undergoes a large-scale conformational change to a conformation where neither the external nor internal cavity becomes accessible to the environment: the occluded-intermediate state (Figure 2c). Subsequently, the transition to the inward-facing state is completed, which predisposes the transporter to substrate and Na⁺ release (Figure 2d). Following the release of the substrate and sodium ion(s) to the cytoplasm, the empty inward-facing transporter (Figure 2e) is presumed to reconfigure back to its outward-facing form, thus completing one transport cycle.

Alternatively, in the outward-facing state, a competitive blocker may bind to the primary site (where the substrate binds) (Figure 2f) or a non-competitive blocker may bind to a secondary site (usually located within the cavity “above” the primary site) locking the transporter in that state and preventing progress through the transport cycle. Inhibitors of transport may also bind to the intracellular (IC) cavity that is exposed in the inward-facing state.

The scheme in Figure 2 is a simplified description of the transport cycle since in many cases the cycle does not merely include the substrate and Na⁺ but other cations and/or anions alike. For instance, in the serotonin and γ -aminobutyric acid transporters, SERT and GAT-1, respectively — which belong to the NSS family — a chloride ion is co-transported with the substrate and Na⁺ ion,^{35,36} but in the neuronal Glu⁻ transporter EAAT3, a potassium ion is counter-transported.¹²

In the following, for clarity, we will distinguish between the local and global structural changes. Generally, the transporter can assume an inward- or an outward-facing state, and in each state, it may assume alternative conformations accessed by structural changes on a smaller scale. In the outward-facing conformation, the aqueous cavity leading to the binding site is exposed to the extracellular medium whereas in the inward-facing one, the binding pocket becomes accessible to the intracellular medium. The passage between the inward- and outward-facing states involves cooperative changes in the overall structure — hence termed “global” — whereas in each state, changes on a smaller scale may occur which cause the binding pocket to become accessible (*open*) or inaccessible (*occluded*) to the inner or outer media — hence termed “local changes”. The diagrams (a), (b) and (f) in Figure 2 represent the outward-facing state, which may assume an

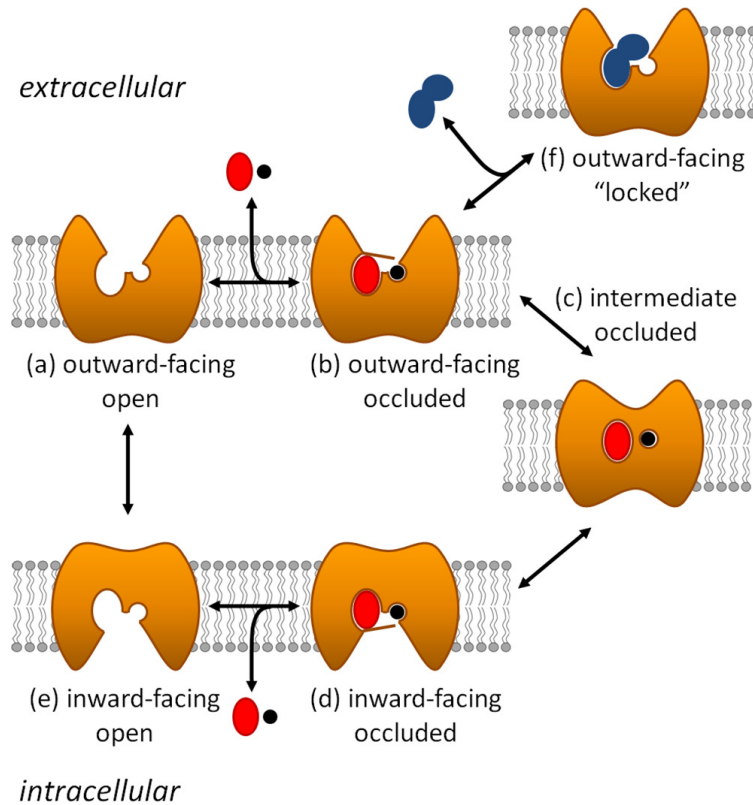


Figure 2. Schematic depicting the general transport cycle in a sodium-coupled transporter. The transporter with the binding site accessible to the EC medium (a) binds the substrate (*red ellipse*) and one or more sodium ions (*black circle*) (b). In the latter conformer, referred to as the outward-facing occluded conformation, the substrate and sodium ion(s) are mostly shielded from the EC medium by a small loop or one or more hydrophobic side chains. Following binding, the transporter shifts to an intermediate occluded state where the substrate and sodium ion(s) are inaccessible from either side of the membrane (c) before undergoing further conformational changes that cause the cavity leading to the binding site to become accessible to the IC medium (d). The substrate and sodium ion(s) are then released into the cytoplasm and the empty inward-facing transporter (e) reorients to face the EC medium again before a new cycle can begin. Alternatively, the transporter may bind an EC competitive inhibitor (*dark blue*) and become “locked” in an open conformation (f) inhibiting the completion of the transport cycle.

open (a), occluded (or closed) (b) or an inhibitor-bound (locked) (f) conformation. Likewise, (d) and (e) refer to the occluded and open forms of the inward-facing state, respectively. (c) represents an intermediate state.

2.2. Balance of forces/potentials across the membrane favors Na^+ inward flow

Two factors govern the movement of ions across selectively permeable membranes: the electric potential, or voltage difference across the membrane, and the chemical potential, or ion concentration gradient across the membrane. The sum of these potentials constitutes the electrochemical

potential. When a Na^+ ion moves from outside to inside the cell, the associated free-energy change due to Na^+ concentration gradient is given by

$$\Delta G_c = RT \ln([\text{Na}^+]_{\text{in}}/[\text{Na}^+]_{\text{out}}), \quad (1)$$

where R is the gas constant and T is the absolute temperature. Under physiological conditions typical of many mammalian cells, $[\text{Na}^+]_{\text{in}} = 12 \text{ mM}$ and $[\text{Na}^+]_{\text{out}} = 145 \text{ mM}$, which leads to $\Delta G_c = -1.5 \text{ kcal/mol}$ at $T = 300\text{K}$, i.e. there is a free energy release of 1.5 kcal/mol accompanying the transport of each Na^+ to the cell interior, assuming that there is no membrane electric potential. On the other hand, the free energy change due to the membrane electric potential (using a resting membrane potential $E = -70 \text{ mV}$ in a typical neuron) is

$$\Delta G_m = FE = -1.6 \text{ kcal/mol}, \quad (2)$$

for the transport of each monovalent cation (e.g. Na^+) from outside to inside the cell. Here F is the Faraday constant. Since both Eq. (1) and Eq. (2) apply to Na^+ ions, the total free energy change ΔG associated with the translocation of one Na^+ is the sum

$$\Delta G = \Delta G_c + \Delta G_m = -3.1 \text{ kcal/mol}. \quad (3)$$

Thus, the inward movement of Na^+ in a typical neuron is energetically favored by 3.1 kcal/mol .

2.3 Sodium ion co-transport as a driving potential for the transmembrane translocation of solutes by secondary transporters

Polar or charged molecules are unable to diffuse across the hydrophobic lipid bilayer due to unfavorable interactions. Instead, they cross the membrane by permeating through membrane proteins such as transporters or channels. The translocation of a solute molecule is even more difficult if its diffusion is an “uphill” process, i.e. against its concentration gradient or the membrane electric potential. A mechanism to accomplish the uphill translocation is to couple the solute transport to the flow of the ion(s) that is favored by the electrochemical gradient. Secondary transporters utilize such electrochemical gradients. The counter- or co-transport of ions (by antiporters or symporters, respectively) drives the translocation of the solute (substrate). For example, as described above, the free energy change generated from the movement of a Na^+ ion from outside to inside the cell is approximately -3 kcal/mol [Eq. (3)]. The transport of three Na^+ ions, for example, would permit the cell to accumulate a higher concentration of solute (e.g. a neurotransmitter such as dopamine or Glu^-) relative to the exterior concentration to counterbalance this potential: under equilibrium conditions, in the absence of other effects and assuming the solute is neutral,

$$RT \ln[S_{\text{in}}]/[S_{\text{out}}] = 3(-3.1) = -9.3 \text{ kcal/mol} \quad (4)$$

which leads to $[S_{\text{in}}]/[S_{\text{out}}] \approx 3 \times 10^6$ at 310 K . Thus, the free energy release associated with the transport of three sodium ions allows for the transport of an uncharged neurotransmitter against a

10^6 -fold concentration increase. In the case of human EAATs, the transport of each Glu^- is accompanied by the co-transport of 3Na^+ and a proton (H^+), followed by the counter-transport of a potassium ion (K^+), such that there is a net influx of two cations.

3. Structural Information

Up until a few years ago, no high-resolution structural data were available for Na^+ -coupled secondary transporters, mainly due to their hydrophobic and dynamic nature, which makes them difficult to crystallize. Recently, however, the crystal structures of several distantly related transporters with bound substrate and/or sodium ions have been resolved (Table 1). Two prime examples, Glt_{ph} and LeuT, both in the outward-facing state, are illustrated in Figure 3. Notably, the

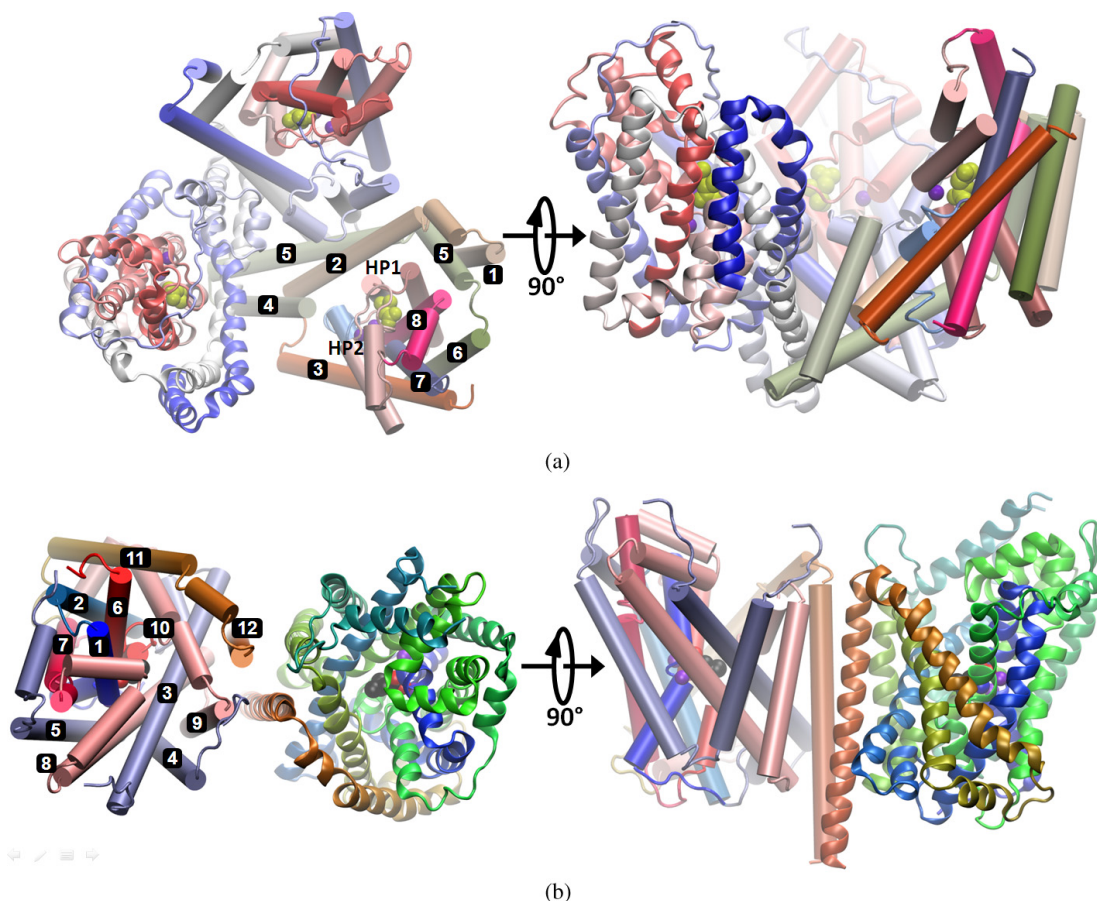


Figure 3. Crystal structures of two widely studied homologs of neurotransmitter transporters, Glt_{ph} trimer and LeuT dimer. The outward-facing states of Glt_{ph} (a) and LeuT (b) are shown here. The structures are viewed from the EC side (left) and through the plane of the membrane (right) together with the bound sodium ions (purple spheres), Asp- (a) (yellow space-filling) or Leu (b) (black space-filling). The structures are generated using the respective PDB files 1XFH and 2A65 and the visualization software *VMD*.⁴¹ For clarity, one of the monomers is shown in ribbon representation in each case, and the remaining, in cylinders.

structures resolved to date capture these proteins in different conformations providing us with full atomic coordinates data on alternative forms visited along the transport cycle depicted in Figure 2. Not only have these structures confirmed previous experimental work, but they have also revealed two main distinct features of this class of transporters: an internal two-fold structural symmetry and a discontinuity of transmembrane (TM) helices at the substrate/ion binding sites.^{10,18–21,28,37–40} Most importantly, they provide important insights into the molecular mechanisms that mediate substrate translocation and permit us to perform structure-based computations toward elucidating time-dependent events.

Symporters that share the LeuT fold exhibit significant commonalities in their core regions' structure and interactions, despite their lack of sequence similarity, which suggests that the LeuT fold encodes a common mechanism of substrate transport. The emerging molecular details about the structure and mechanism of these transporters have consolidated them into one main structural family. Below we present more details on the Glt_{ph} and LeuT structures.

3.1 Structure and topology

Glt_{ph} is a homotrimer. The three subunits form a bowl-shaped concave basin towards the EC side (Figure 3a). Each subunit is comprised of eight TM helices, TM1-TM8, and two helical hairpins, HP1 and HP2. These structural elements are organized into an N-terminal, outer cylinder region made up of TM helices TM1-TM6, and a C-terminal core comprised of TM7, HP1, HP2 and TM8 (Figure 4a). Within each monomer, the core region encompasses the elements of substrate binding and the transport machinery whereas the outer region (known as the scaffold) provides stability and interacts with the two other subunits.²⁰

In the case of NSS family and the families with a similar structural fold, the transporters form homo-dimers or -trimers in the membrane upon crystallization. These oligomeric forms are, at least for many of them, the physiological states while the monomer is the functional unit. The monomer is composed of 11-14 TM helices and the common core is formed by 10 TM helices, the numbering of which can vary: in LeuT and Mhp1 they are helices 1 to 10 (Figure 4b), in vSGLT, 2 to 11, and in BetP, 3 to 12. The core, in the case of LeuT for example, can be divided into two structurally symmetric "halves", or repeats: TM1-TM5 and TM6-TM10. The first helix of each repeat contains a break (unwound portion) about halfway across the membrane. This break exposes backbone polar groups that interact with the substrate and the co-transported sodium ion(s) (Figure 4b).

Only recently, after the elucidation of a number of high-resolution structures did we gain deeper insights into the mechanisms of substrate transport by Na⁺-coupled secondary transporters.^{42,43} These structures reveal that transporters may indeed share similar local motifs, even if they have different folds and topologies. LeuT (and symporters with a similar fold) and Glt_{ph} as well as the sodium/proton antiporter, NhaA, share the internal pseudo-symmetry and the breaks in the TM helices.

3.2 Substrate and sodium binding

In Glt_{ph}, the substrate binding site in each subunit is covered by the loops of HP1 and HP2. There are several conserved residues within 5–7 Å of the substrate binding site. These residues include

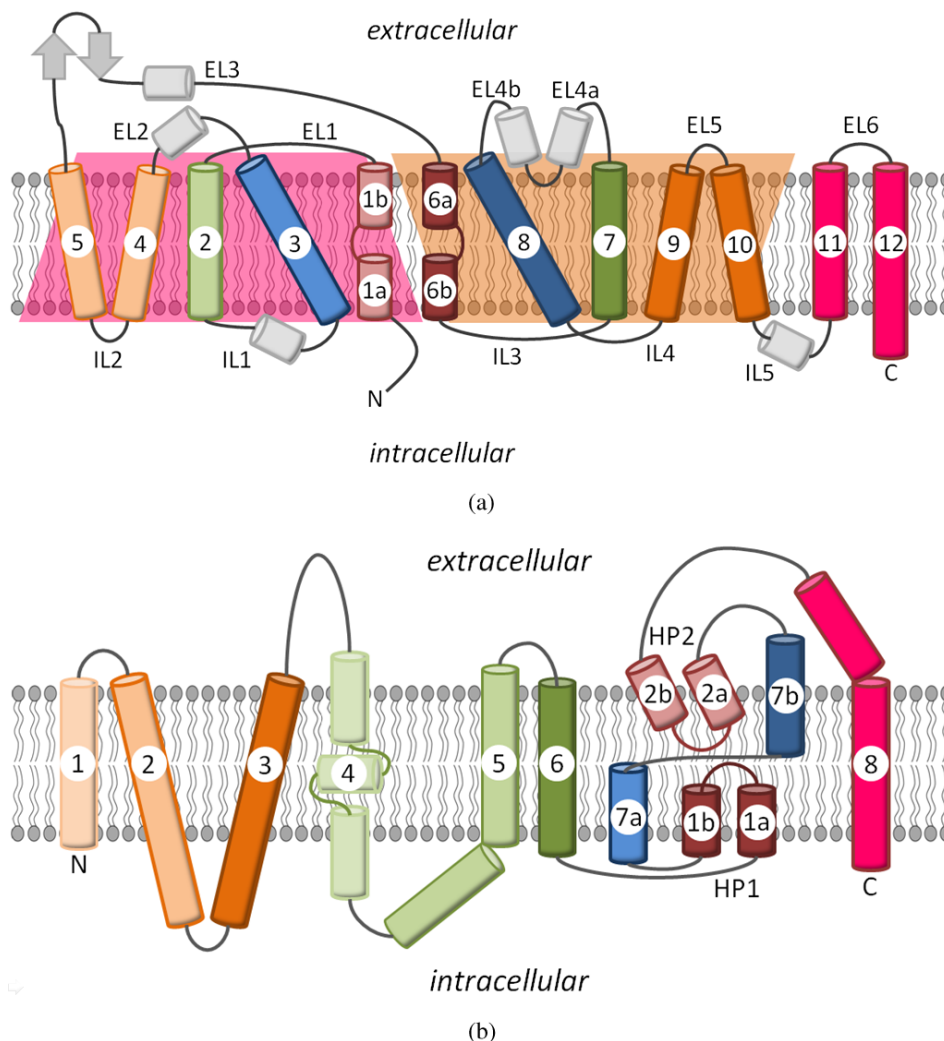


Figure 4. Schematic description of the topology of Glt_{ph} and LeuT. Helices are shown as cylinders and TM helices are numbered. The substrate and sodium ions (yellow rectangle and circles, respectively) are shown at the binding site of Glt_{ph} (a) and LeuT (b). In (b), the two pseudo-repeats, TM helices 1-5 and 6-10, are shaded (pink and orange, respectively). Extracellular and intracellular loops are labeled as EL and IL, respectively, and numbered according to their sequence position.

the highly conserved serine motif (Ser277-Ser278-Ser279) on the HP1 loop, two glycines (Gly354 and Gly357) on the HP2 loop, the NMDGT motif between Asn310 and Thr314 on TM7, Asp394, Arg397, Thr398 and Asn401 on TM8. Of these residues, Gly354 and Gly357 are considered to coordinate one of the two bound Na⁺ ions (Figure 5a). In the higher resolution Asp-bound outward-facing structure,¹⁸ a Na⁺ ion (referred to as Na2) is bound close to this position, interacting with Thr352, Ser349 and Ile350. Additionally, there is a second Na⁺ ion binding site (Na1),

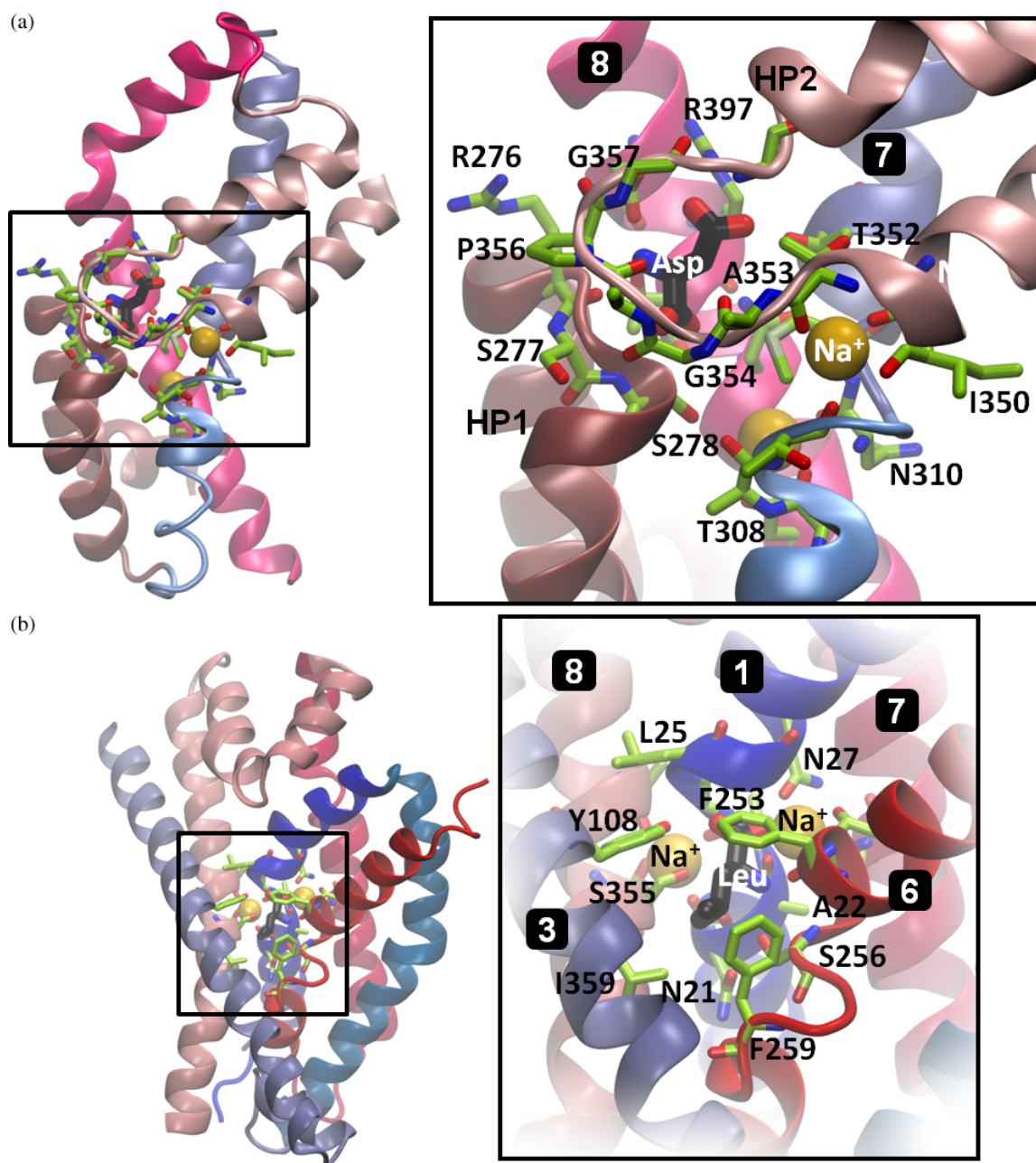


Figure 5. The substrate binding site in Glt_{ph} and LeuT. A close-up on the core domain of Glt_{ph} composed of HP1, HP2, TM7 and TM8 (a), and the substrate- and Na⁺-binding site of LeuT between TM1, TM3, TM6, TM7 and TM8 (b). The structures are viewed through the plane of the membrane. The substrate is shown in black in each case, and the bound Na⁺ ions in yellow. The residues interacting with the substrate are shown in green stick representation. The ribbon diagrams were generated using the same PDB structures and software as those used in Figure 3.

located deeper in the core near Gly306 and Asn310 on TM7 and Asn401 and Asp405 on TM8 (Figure 5a).

In the case of secondary transporters with the LeuT fold, as the identities of the substrate vary among and within the families, so do the residues that coordinate them. The substrate may be a biogenic amine in the case of NSS family members, a sugar in the case of an SGLT (SSS family) or a nucleobase in the case of Mhp1 (NCS1 family). The substrate is usually located at the center of each monomer, halfway across the membrane and at the interface between the two structural repeats (Figures 3b and 5b). The TM helices taking part in binding the substrates, and their spatial organization, however, are similar in most cases: TM1, 3, 6 and 8 in LeuT and Mhp1, TM2, 3, 7, 8 and 11 in vSGLT (the counterparts of TM1, 2, 6, 7 and 10 in LeuT and Mhp1); and TM1, 3, 6, 8 and 10 in the structurally related but not sodium-coupled antiporters AdiC1 and CaiT.³⁹ Figure 6 panels (a) and (b) illustrate the close superposition of these equivalent helices for LeuT, Mhp1 and vSGLT.

Two sodium ion-binding sites have been identified for the transporters with the LeuT fold, which, on the basis of those initially identified in the LeuT structure, are referred to as: (1) Na1, observed only in the crystal structure of LeuT so far, where Na^+ is coordinated by residues on TM1, TM6 and TM7, and by the carboxyl group of the substrate (Figure 5b), and (2) Na2, which appears to be a more general site, observed in LeuT and proposed in Mhp1 and vSGLT. In the latter two structures, Na2 is likely to be coordinated by residues on TM1 and TM8, as illustrated in Figure 6c. In the case of BetP, even though the residues observed at the Na2 site are on TM1 and TM5, the binding cavity is lined by residues on TM8.

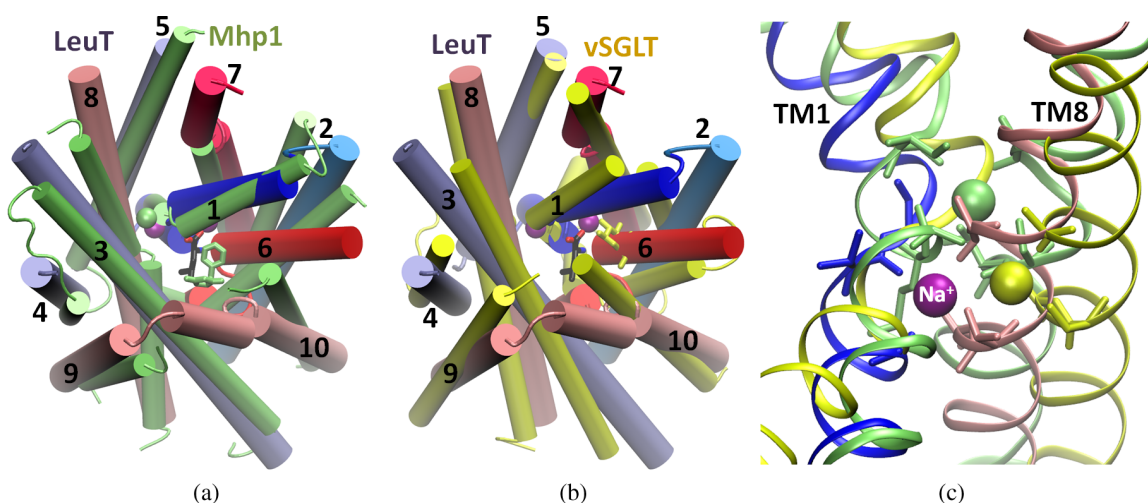


Figure 6. Superposition of three members of NSS family of transporters. Crystal structures of LeuT in the outward-facing state (blue and red) superposed on that of (a) Mhp1 (lime green) in the outward-facing state, and (b) vSGLT (yellow) in the inward-facing state. The molecules are viewed from the EC side (a and b), and through the membrane zooming in on the sodium-binding site equivalent to that of Na2 in LeuT (c). The substrates (licorice) and sodium ions (spheres) are colored with respect to the transporters. TM helices are numbered according to LeuT. Only the 10 core helices are shown here.

The fact that sodium designated as Na1 is directly coordinated by the negatively charged carboxyl group of the substrate (regardless of whether it is leucine, glycine, alanine, or otherwise)³⁸ suggests a direct coupling and possibly a cooperativity between the substrate and sodium in binding and/or transport. In contrast, the second sodium ion (Na2) seems to be required for the structural stability of the binding pocket and the increased selectivity for Na⁺ at Na1.⁴⁴ Computational approaches have shown that in the substrate-occluded conformation of LeuT, there is no preference for Na⁺ over the larger K⁺ at Na1, where Na⁺ is coordinated by six ligands including the carboxyl group of the substrate, and the same is true for Na2 where Na⁺ is coordinated by five neutral ligands. In contrast, only modest preference for Na⁺ over the smaller Li⁺ was observed at both sites using the same approach based on free energy calculations.⁴⁵

It is interesting to note that TM1 and TM6 in LeuT, Mhp1 and AdiC1, and their counterparts in vSGLT and CaiT, are partially unwound (or broken) (see the topology diagram for LeuT in Figure 4b). These particular regions contain several “frustrated” backbone carbonyl and amino groups that lack hydrogen bond-forming partners, and as such, serve as avid binding sites for substrate and ion binding. Notably, the TM7 and TM8 helices in the core domain of Glt_{ph} also have such partially unwound segments containing highly conserved residues (e.g. the NMDGT motif) that play a critical role in binding the substrate or cations, consistent with the same “design principle”. However, this mechanism of substrate binding may not hold for all conformational states of the transporters. In the crystallized intermediate occluded conformation of BetP (see Table 1), for instance, the substrate is liganded by residues on the intact helices TM4 and TM8, which are equivalent to TM2 and TM6 in LeuT.¹⁰

4. Molecular Mechanisms Revealed by Structure-Based Modeling and Computations

With the elucidation of LeuT, Glt_{ph} and other Na⁺-coupled transporters' structures (Table 1), several structure-based computational studies have been launched in different laboratories, which are now nicely complementing experimental findings in helping us gain insights into the transport mechanisms and visualize time-dependent events at the atomic scale. It is now clear that the description of the transport mechanism in terms of only two macrostates, inward-facing and outward-facing, is an oversimplification. In principle, transporters — like all other proteins — are subject to a multitude of conformational motions that enable their activity. A protein of *N* interaction sites enjoys 3*N*-6 internal degrees of freedom; thus, its equilibrium motions are described in terms of 3*N*-6 collective mode directions that form an orthonormal basis set. Each mode has its own “time constant” and “mechanism” described by the respective eigenvalue and eigenvector of the covariance matrix for the fluctuations of interaction sites. It is customary to describe this complex space of conformational changes in terms of a few kinetic parameters, e.g. by adopting single-, bi- or tri-exponential time-dependent functions for describing the time evolution of experimentally detected events. However, in a strict sense, the function involves an ensemble of motions.

Of the broad spectrum of motions accessible to transporters, state-of-the-art molecular dynamics (MD) simulations can explore those occurring on the order of nanoseconds; perhaps those up to tenths of microseconds with adequate computing resources. Such motions typically involve

local changes in structure. Examination of longer time, larger-scale movements, or so-called global motions, on the other hand, requires the adoption of simplified models. Simplified models such as *elastic network models* (ENMs) permit us to learn about potential cooperative movements (e.g. domain/subunit rearrangements) that involve the entire molecule, at the cost of losing atomic level accuracy.⁴⁶ In many cases, the first step before launching the simulations is to model the structure, in the absence of available experimental structure. The most feasible way to achieve this goal is *comparative/homology modeling*, provided that a sequence homolog of the investigated protein has been structurally resolved.

Therefore, structure-based computations consist of three major groups: (1) MD simulations for exploring local events in the nanoseconds regime, e.g. gating, substrate/ion binding or release, or fluctuations between open and occluded forms in either the outward-facing state or the inward-facing state, i.e. the horizontal steps in the transport cycle depicted in Figure 2, but not the passage between the two states (vertical steps), (2) homology modeling for predicting the structures of family members not resolved to date, or for predicting the alternative (functional) structures of a known transporter, using as template the known structure of a family member, and (3) coarse-grained approaches, usually based on simplified models such as the ENMs and normal mode analysis (NMA), toward exploring the passage between outward-facing and inward-facing states (the vertical steps in Figure 2). Results from these three respective groups of computations will be summarized in the Sections 4, 5.1 and 5.2, respectively. Results in Section 4 will be presented in two subsections: Section 4.1 for Glu⁻/Asp⁻ transporters, and Section 4.2 for NSS family members or their structural homologs.

4.1 Local Motions and Substrate/Sodium Interactions in Glutamate Transporters

4.1.1 Gate opening in the outward-facing state of *Glt_{Ph}*

The resolution of the X-ray structure of the archaeal Asp⁻ transporter *Glt_{Ph}* provided a major breakthrough in understanding the structural underpinnings of the transport mechanism at the molecular level.²⁰ Extensive MD simulations performed with this outward-facing structure in the presence of explicit lipid and solvent molecules revealed various aspects of the substrate recognition and binding events of the transport cycle.^{47,48}

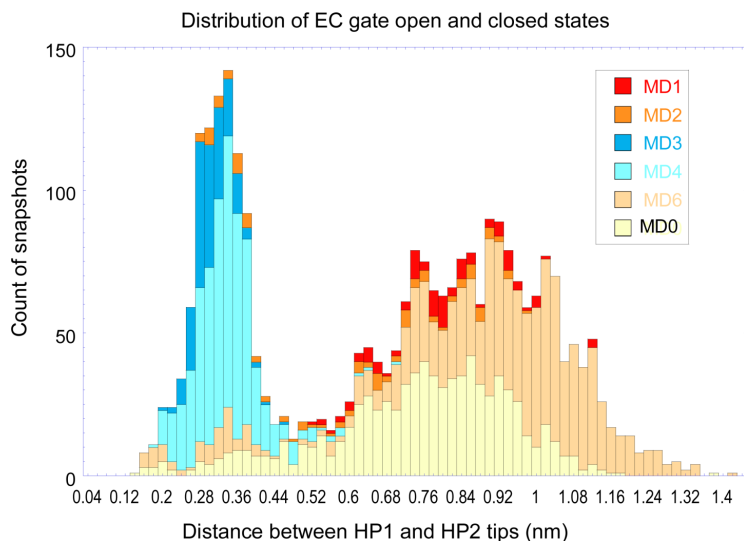
First, the simulations performed in the absence of substrate exhibited striking motions in the HP2 loop of the protein. This loop has a tendency to open up within a couple of nanoseconds in one subunit, followed by the opening up of the HP2 loop in one of the two other subunits within approximately 15 ns. The opening of the HP2 loop exposes several highly conserved charged/polar residues (e.g., Arg276, Ser277-Ser278-Ser279, on HP1 and the N310-MDG-T314 motif on TM7) at the substrate binding site to the EC region. The exposure of these residues with high-affinity to attract the substrate from the aqueous environment seems to be a pre-requisite for substrate binding. Simulations suggest that HP2 acts not only as an EC gate but also as an attractor driving the diffusion of the substrate from the aqueous basin towards the binding site, as evidenced by the involvement of HP2 glycines in the initial recognition events.

The opening of the HP2 loop in the fast regime observed by MD simulations supports the view that the transporter core domain possesses an intrinsic ability to open an EC gate for substrate entry. This propensity is supported by the X-ray structure of Glt_{ph} in a complex with the non-transportable blocker *DL-threo-β*-benzyloxyaspartate, where HP2 is blocked in an open conformation.¹⁸

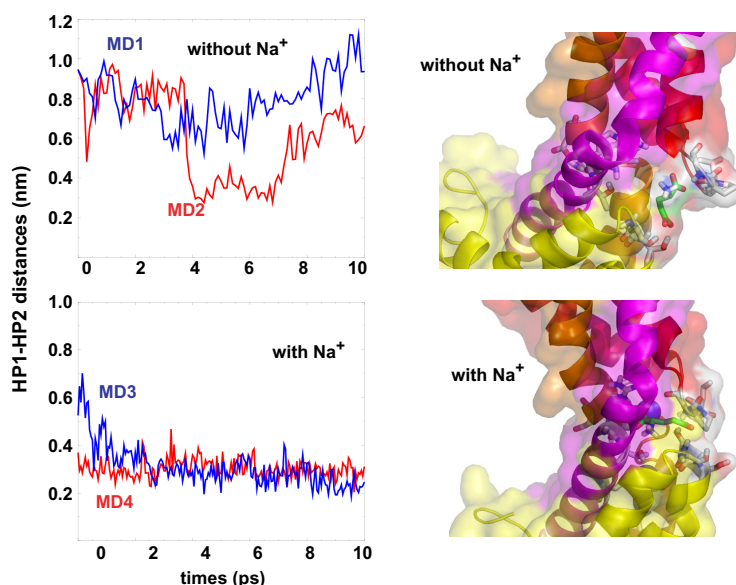
Second, a series of simulations have been performed, with and without substrate, in the absence and presence of sodium ions, to examine the effects of the substrate on the binding pocket.⁴⁷ Figure 7a displays a cumulative histogram derived from the analysis of the HP2 motions in these MD runs, MD0-MD6. The distance between two residues, Ser278 and Gly354 (Figure 5a), at the respective tips of HP1 and HP2 was monitored therein as basis for probing the state of the EC gate. In all runs, the HP1 loop was observed to be highly stable and almost rigid while the HP2 loop (EC gate) would always open up in at least one of the subunits, irrespective of whether the substrate was bound or not. The two peaks in the histogram indeed correspond to the open and closed conformations sampled by the EC gate. The open conformation exhibits a broader distribution consistent with the high conformational variability of the HP2 loop in this conformation, while the closed conformation exhibits a sharper peak centered around 3 Å. These simulations thus confirmed that the HP2 hairpin serves as an EC gate in the outward-facing state, in either substrate-bound or -unbound forms.

4.1.2 Role of Na^+ ions in stabilizing the closed conformation of the EC gate in the substrate-bound outward-facing Glt_{ph}

The data compiled in Figure 7a refer to multiple runs conducted under different conditions: In the absence of the substrate (empty conformer, outward-facing state), the Glt_{ph} subunits exhibit a high tendency to sample the open state (MD0 and MD6), and this tendency is maintained, albeit to a lesser extent, in the presence of bound substrate (occluded form, outward-facing state) (MD1 and MD2). Binding of sodium ions, on the other hand, strongly favors the closed conformer. The stabilizing role of Na^+ ions at the binding site is clearly evident in the runs (MD3 and MD4) conducted in the presence of bound Na^+ ions. Panel (b) in Figure 7 compares the time evolution of the distance between the HP1-HP2 tips in different runs (left) and displays snapshots from the runs conducted without (top) and with (bottom) sodium ions (right). The results clearly demonstrate the tight interaction of HP1 and HP2 tip residues in the presence of Na^+ ions. This interaction keeps the EC gate closed, in the occluded (outward-facing) conformation, suggesting the role of at least one sodium ion at the binding site as “gate-keeper” in addition to its role in assisting substrate transport. Notably, the substrate molecule located within the EC basin is observed to readily recognize the binding site, provided that the HP2 loop of a given subunit opens up, and diffuses toward that particular subunit to enter the binding site and interact tightly therein with the conserved polar residues on HP1, TM7 and TM8.⁴⁷ Simulations showed that once the substrate enters the binding site, it remains tightly bound for the entire duration of the simulation (40–50 ns), without exiting the transporter. The translocation indeed requires a global structural change to the inward-facing structure (see Section 5), which is a several orders of magnitude slower process currently beyond the time scale of MD simulations.



(a)



(b)

Figure 7. Local motions observed in MD simulations of Glt_{pn} outward-facing state. Panel (a) shows the occurrence of two conformers, open and closed, for the EC gate (HP2 loop). The distance between the residues Ser278 and Gly354 at the HP1 and HP2 tips (Figure 5a), respectively, exhibited a bimodal distribution in multiple simulations (MD0-MD6), indicative of the two distinctive states of the EC gate. For details of these simulations see Ref. 47. The narrow peak at shorter separation corresponds to the closed conformations, and the broader peak around 0.9 nm, to open conformations. The runs MD3 and MD4 (cyan and blue) were conducted in the presence of bound Na⁺ ions; and all other runs, without Na⁺ ions. Panel (b) shows the role of Na⁺ ions in stabilizing the closed conformations of the EC gate. The curves on the left show the time evolution of HP1-HP2 tip distances in MD1 (blue) and MD2 (red) top panel, and MD3 (blue) and MD4 (red), bottom panel. The diagrams on the right display the substrate-protein interactions at the binding site in an open (top) and closed (bottom) conformation of the EC gate. In both panels, the substrate is shown in stick representation, with the backbone colored green; the Na⁺ ions are shown as purple spheres; HP1 and HP2 are colored yellow and red, respectively; TM7 and TM8 are orange and magenta; and the residues interacting with the substrate are shown in stick-representation.

4.1.3 Na^+ and substrate release by Glt_{ph} in the inward-facing state

The mechanism of release of the substrate into the IC region remained unclear until the recent determination of the inward-facing structure of Glt_{ph} .¹⁹ The popular hypothesis has been to view the two helical hairpins, HP2 and HP1, in the core domain of each subunit, as the respective EC and IC gates for substrate entry and release. The former has indeed been confirmed by both MD simulations^{47,48} and experiments^{18,20} to serve as an EC gate (Figure 7). The latter (HP1), on the other hand, could not be computationally confirmed up until now, due to the absence of an atomic structure for the inward-facing structure, which could serve as a starting point for MD simulations. With the recent elucidation of this structure by Boudker lab, we have been able to gain insights into the mechanism of substrate release. The emerging sequence of events that control Asp^- release to the cytoplasm is the following. First, in parallel with the behavior in the outward-facing form, the HP2 loop is by far more flexible than the HP1 loop at early stages of simulations. Figure 8 displays snapshots from an unbiased MD run in the presence of explicit water and lipid molecules, where the opening of the HP2 loop, the accompanying dissociation of Na_2 , and ensuing solvation of the binding site may be clearly seen. Notably, the release of Na_2 further destabilizes the HP2 loop, and the resultant enhanced fluctuations facilitate a more massive influx of water molecules, which effectively compete with the polar and charged residues that ligate the bound substrate, and lead to the dislodging of Asp^- from its binding site (Figure 8). Yet, the release from the binding pocket also requires the opening of the HP1 loop. In fact, as shown in Figure 9, persistent hydrogen bonds with the conserved amino acids S277 and S278 at the HP1 loop prevent the substrate dissociation (at 44 ns) and even drive the substrate back near the binding pocket (at 45 ns). This momentary setback in substrate release is however overcome at 49 ns where the disruption of a hydrogen bond with S277 remains as the last step to complete dissociation. Notably, the inner sodium ion (Na_1) is observed to remain bound and almost fixed during all these events.

Thus, substrate release necessitates both the fluctuations in HP2 and the opening of HP1. Although both HP1 and HP2 share a helix-turn-helix motif, the identities of the conserved amino acids that comprise the loops are very different.²⁰ The HP1 loop is composed of four polar/charged residues (Arg276, Ser277, Ser278, and Ser279), whereas the HP2 loop is composed of hydrophobic side-chains of (Ala353, Ala358, and Val355), four glycines (351, 354, 357, and 359) and Pro356. Furthermore, the chemical identity of the HP1 loop residues is consistent with their strong interactions with the substrate: the side-chains of Ser277 and Ser278 remain hydrogen-bonded to the substrate and Arg276 is locked in a salt-bridge with the side-chain of Asp238 of TM8 during a large portion of the simulations. The floppier, hydrophobic chemical identity of the HP2 loop, therefore, makes this loop intrinsically predisposed to undergo larger magnitude motions, but final substrate release is not achieved until there is a conformational change (opening) in HP1 loop as well.

The intrinsic ability of Glt_{ph} to sample the various conformational states to facilitate both substrate binding and release, which is enabled by the global change in structure from outward- to inward-facing, highlights the adroit dynamic functionality of the HP1 and HP2 loops in assisting the transport of amino acids during synaptic transmission.

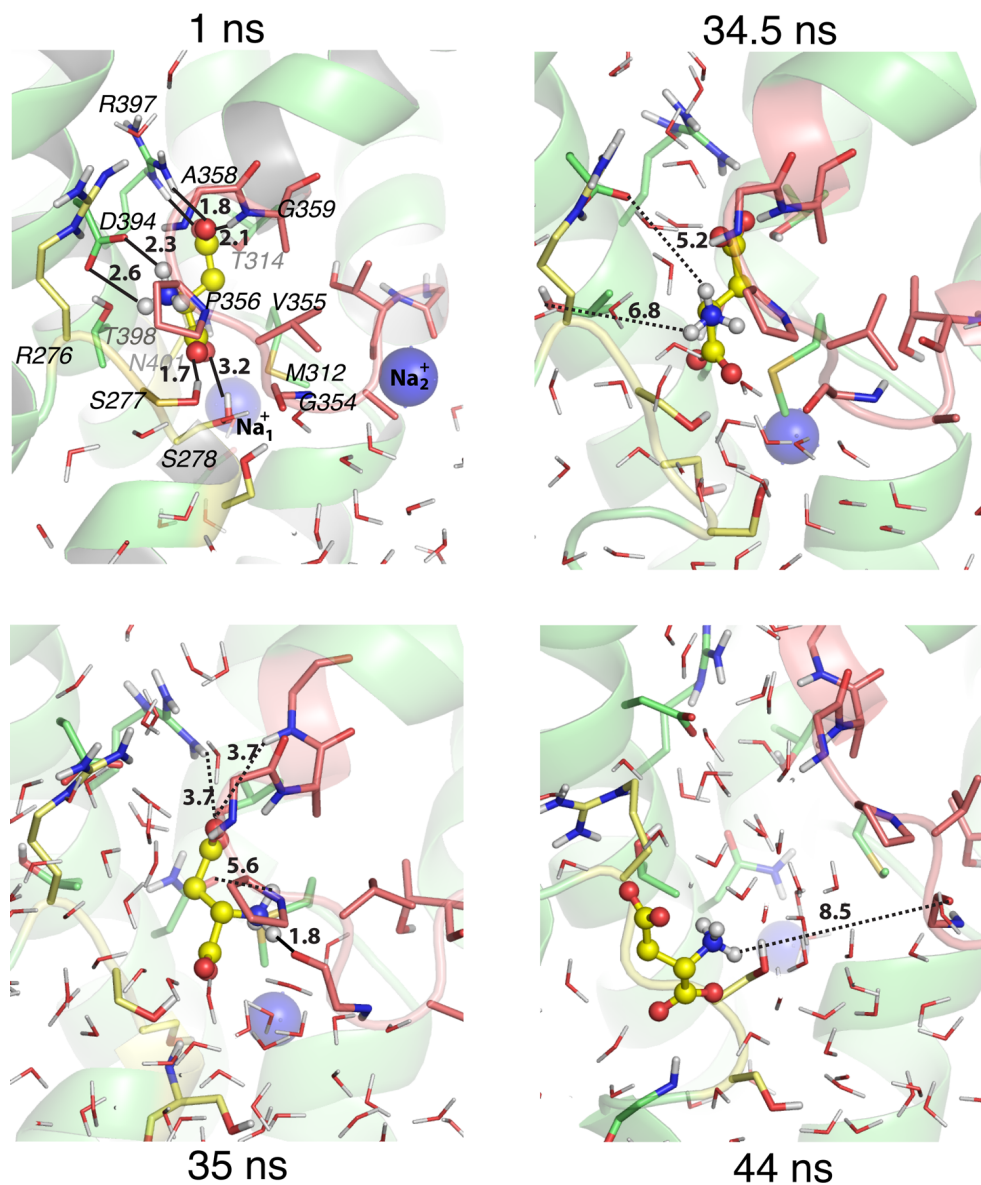


Figure 8. Succession of events leading to the dislocation of substrate in the inward-facing state of Glt_{ph}. Distances between substrate atoms and the closest atoms on the labeled amino acids are reported in Ångstroms. At $t = 1$ ns, the bound substrate is sequestered from the IC solvent by the closed loop conformation of HP2 and HP1. At $t = 15$ ns (not shown), Na⁺₂ begins to dislodge from its binding site. Snapshots at 34.5 and 35 ns demonstrate the significant change in the conformation of the substrate within 0.5 ns, induced by the severed hydrogen bonds to Asp394 and Arg397, which arise from binding site solvation following the opening of the HP2 loop. At $t = 44$ ns, the substrate is dislodged from the binding cavity. Note that the substrate is completely dissociated from HP2, as evidenced by the increase in the distance between the Asp- NH group and HP2 Gly354 backbone hydroxyl from 1.8 Å at $t = 35$ ns to 8.5 Å at $t = 44$ ns, while there is a substrate-protein hydrogen bond (1.8 Å) between the Asp- β -carboxylate oxygen and the hydroxyl group of Ser277 on the 3-Ser motif at the HP1 loop.⁴⁹

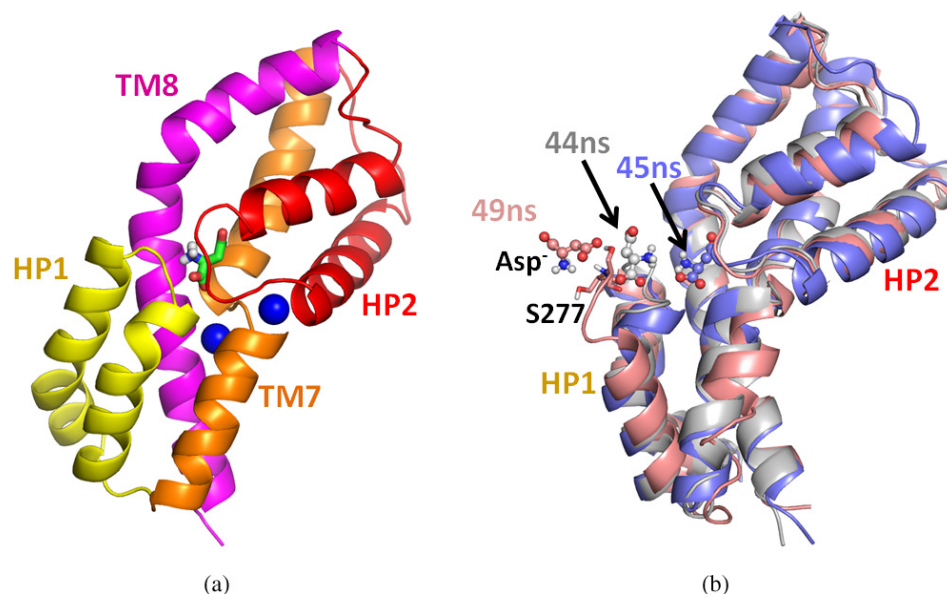


Figure 9. Last step of aspartate transport cycle by Glt_{pn} : involvement of HP1 in the final release of substrate in the inward-facing state. Panel (a) displays the original structure of the core domain in one of the subunits, color coded by the secondary structural elements, including both the bound substrate and two sodium ions. Panel (b) displays three snapshots of the same subunit taken at 44, 45 and 49 ns, succeeding the influx of water molecules and dislocation of substrate (see Figure 8). The substrate which was partially dissociated at $t = 44$ ns is attracted back toward the binding pocket at 45 ns, but moves back towards the cytoplasm this time enabled by the substantial “opening” of the HP1 loop while the hydrogen bond between Asp- β -carboxylate oxygen and Ser277 hydroxyl group is maintained. The structure in panel B is slightly rotated along the vertical axis to allow for better visualization of the opening of HP1 loop.

4.2 Conformational dynamics of NSS family members and their structural homologs

The elucidation of the crystal structure of either the substrate-bound or empty conformers of transporters such as LeuT, Mhp1, vSGLT and AdiC1 has provided insights into local motions that take place in this particular (LeuT fold) family of transporters upon binding the substrate (and/or Na^+). Despite some commonalities in their local motions, a single unifying mechanism cannot yet be inferred, suggesting that on a local scale the particular types of motions depend on amino acid identities and specificities. This is in contrast to global motions that are predominantly defined by the fold/architecture (and therefore amenable to coarse-grained analyses), irrespective of the amino acid sequence. In this section (4.2), we focus on these local motions (mainly involved in substrate/ Na^+ binding or release in a given state), and in Section 5 we will examine the global motions (transitions between inward- and outward-facing states) undergone by secondary transporters.

4.2.1 Molecular dynamics of transporters that share the LeuT fold

With regard to local changes near a given state, a comparison between the occluded and open conformers of the outward-facing state of LeuT (based on the crystal structures of the substrate or

competitive inhibitor-bound states, respectively) shows that more significant movements occur in TM helices 1b, 2a and 6b which rotate by ~ 9 degrees to partially close the external cavity.³⁸ In Mhp1, the major change seen is bending of the N-terminal part of TM10⁴⁰ and in AdiC1, which is not sodium-coupled, TM2, TM6a and TM10 are repositioned following substrate binding, with the most prominent motion occurring in TM6a that rotates by about 40 degrees.⁵⁰ Even though these motions are not mutually exclusive when the overall changes in structure from the outward-facing empty state to the inward-facing one are taken into consideration, they do necessitate caution before assuming a general mechanism of conformational change induced upon substrate binding/unbinding in the LeuT fold family.

Several studies have investigated the free energy of binding and the specificity of interactions at the sodium and substrate-binding sites in NSS family members. These include studies performed on the LeuT structure itself^{51,52} as well as LeuT-based homology models of the dopamine and the γ -aminobutyric acid transporters (DAT and GAT-1, respectively).⁵³⁻⁵⁵ Such studies proved to yield good agreement with experimental data in general.^{53,54} It should be noted that with regard to the energetics of binding, these studies have used as a structural template an occluded conformation of the transporter (in the outward-facing state), which may slightly differ from the empty conformation that is recognized by the substrate and Na⁺, as indicated by the different substrate- and inhibitor-bound structures of LeuT.³⁸ Even though the changes between these two conformers may be small in terms of backbone structural deviations, they may still affect the calculated free energies of binding and specific interactions which depend on the detailed geometry of the local environment.

Another common approach has been to conduct steered MD to analyze translocation events that are beyond the time scale of conventional MD.^{30,56-58} Again, caution should be exercised in interpreting the binding/unbinding pathways observed upon application of such external forces. A foreseeable “red flag” would be the application of energies (or pulling forces) much higher than that required for the physiologically relevant conformational changes, which would result in unrealistic events or deformations. To alleviate such effects, it is important to adopt small pulling forces and/or rates of deformation. Yet, such simulations are resorted to in the interest of observing local events relevant to the transport of substrate and suggesting new experiments to test or validate the observed mechanisms. A successful application to LeuT revealed, for example, the existence of a second binding site, termed S2 and located ~ 11 Å “above” the primary site, where the substrate settled while being pulled away from its original binding site towards the EC region.^{56,58} Notably, the S2 site has been observed by experiments to serve as an antidepressant (and detergent) binding site.^{37,59,60} These studies suggest that binding of a second Leu to S2 might promote Na⁺-coupled symport, whereas inhibitor (or detergent) binding to the same site leads to a functionally blocked form.^{58,60}

4.2.2 Spontaneous release of Na⁺ and dislodging of substrate observed in MD simulations of galactose transporter vSGLT

We recently performed a series of molecular dynamics (MD) simulations using the crystal structure of the sodium/galactose symporter (vSGLT).³⁰ This particular structure²⁸ has been reported as the inward-facing, occluded form (Figure 2). Whereas a bound galactose molecule was clearly

discernible in the substrate-binding cavity, no sodium ion was observed in this particular structure. A putative Na^+ -binding site was proposed based on the structural homology between vSGLT and LeuT, the sequence similarity among members of the SSS family and mutational studies.⁶¹ Accordingly, the putative Na^+ site would be accessible to the IC medium, but the substrate would be occluded from the IC medium.²⁸ Investigating the conformational dynamics of this structure via MD simulations showed that a Na^+ ion placed at this putative location would form competing interactions with residues on TM2 and TM9 (the counterparts of TM1 and TM8 in LeuT) and escape from the binding site within nanoseconds to migrate to the IC medium with the help of Asp189, located on TM6 (equivalent to TM5 in LeuT (Figures 10a–10c)).^{29,30}

These MD simulations further showed that even though the substrate was mostly shielded from the IC by an aromatic side-chain (Tyr263), it was accessible to water molecules that entered the binding site. The substrate exhibited significant rotational mobility within the binding site and formed versatile interactions with the protein (Figures 10d–10e). This is in contrast to the tightly-bound Leu and two Na^+ ions in the outward-facing occluded state of LeuT (Figure 4b).^{44,56}

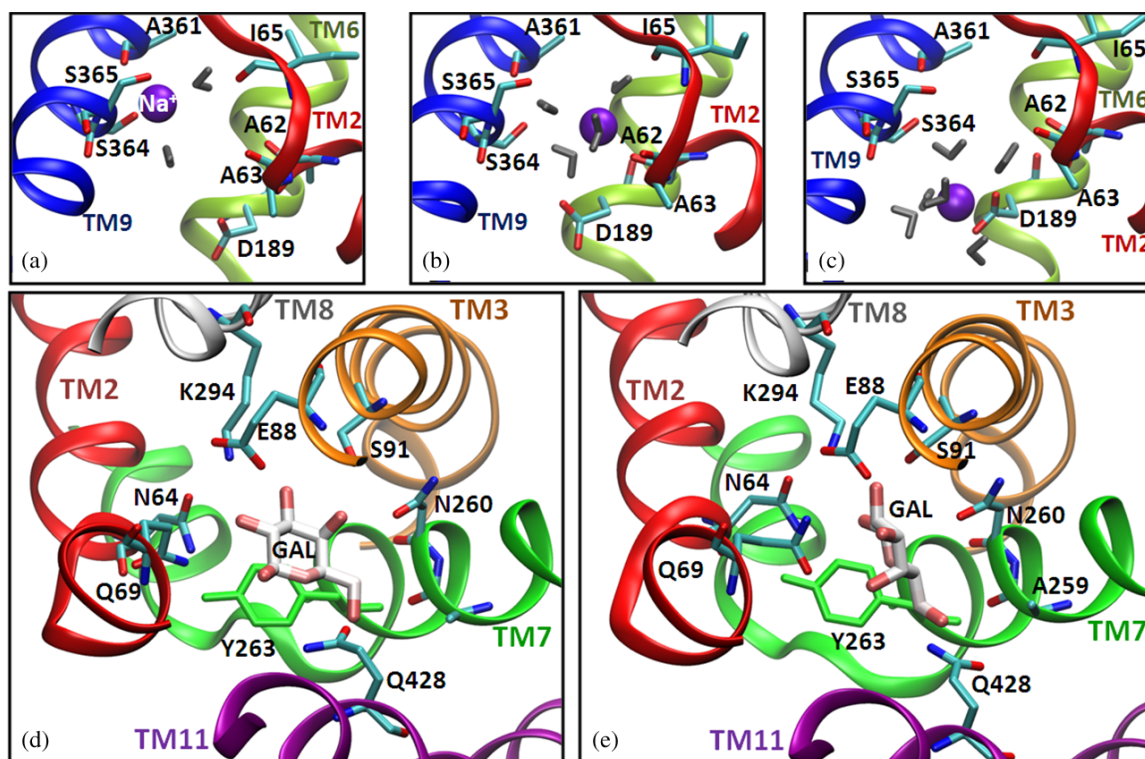


Figure 10. Mobility and interactions of sodium ion and galactose at the binding site of vSGLT. (a–c) Snapshots illustrating the time evolution of the coordination of the sodium ion Na^+ (purple sphere) in vSGLT taken at 1, 5 and 13 ns (a–c, respectively). The Na^+ site, viewed through the plane of the membrane, is shown together with the interacting residues on TM9 (blue), TM2 (red) and TM6 (green) and water molecules (gray). (d–e) Snapshots of the galactose binding site, viewed from the external side, at 10 and 25 ns, respectively. Tyr263 lying between galactose and the IC medium is shown in green. Water molecules interacting with the galactose have been omitted for clarity. See Ref. 30 for more details.

5. Transitions between Inward- and Outward-Facing States Explored by Computational Analyses

5.1 Structure prediction via homology modeling based on structural symmetry

The inverted structural repeats in Glt_{ph} and LeuT have been used to develop homology models for the inward-facing states of Glt_{ph}⁶² and LeuT⁶³ based on the outward-facing crystal structures. We present the results for the respective cases in Sections 5.1.1 and 5.1.2.

5.1.1 Modeling of Glt_{ph} in the inward-facing state based on the outward-facing structure

As described above, each Glt_{ph} subunit is composed of two domains, N-terminal (TM1-TM6) (scaffold) and C-terminal (HP1-TM7-HP2-TM8) (core). Each of these domains is in turn composed of two structural components, also called topological repeat units, which have been noted to be symmetrically arranged with respect to each other in the 3D structure of the particular domain. Thus, each subunit is composed of four topological units overall, as described in Figure 11a. In the N-terminal domain, the helices TM1-3 exhibit an inverted symmetry with respect to TM4-6, and in the C-terminal domain, HP1-TM7 is symmetrically related to HP2-TM8. The two substructures of the scaffold can be closely superimposed onto each other, after two rigid-body rotations of one of them by ~180 degrees as shown in Figure 11b. Likewise, a similar type of superposition is obtained for the core domain. A homology model for the inward-facing state of Glt_{ph} has been generated⁶² by joining the inverted topological repeats, that is, by merging inverted cores 1 and 2 and scaffolds 1 and 2 (note that Figure 11b shows the inversion of core 2 and scaffold 1, only, and similar operations were performed for core 1 and scaffold 2). This resulted in the core-domain moving ~25 Å toward the cytoplasmic region, relative to the outward-facing conformation (Figure 11c). The homology model thus predicted proved to agree very well with the independently resolved structure of Glt_{ph} in the inward-facing state,¹⁹ in support of the alternative access mechanism for substrate transport.

Notably, the Asp⁻ molecules embedded in the binding pocket of each of the three core domains are readily “lifted” to a position closer to the cytoplasm upon the *en bloc* translation of the core domain toward the cytoplasm. The “lift-like” movement of the core domain is accompanied by a radial movement of the three subunits around the cylindrical symmetry axis to restrict the access from the EC region to the originally exposed aqueous basin, while facilitating the exposure of the “translated” binding pocket to the cytoplasm.

5.1.2 Modeling of LeuT in the inward-facing state based on known outward-facing structure

Unlike the Glt_{ph} fold, where high-resolution crystal structures have been determined for both the outward- and inward-facing conformations, the LeuT structure has been resolved in the outward-facing form only. Among other Na⁺-coupled secondary transporters found by X-ray crystallography to share the LeuT fold (Table 1), Mhp1 is the only one captured in both the outward-facing (occluded and open)⁴⁰ and inward-facing⁶⁴ forms.

Sodium-coupled Secondary Transporters

221

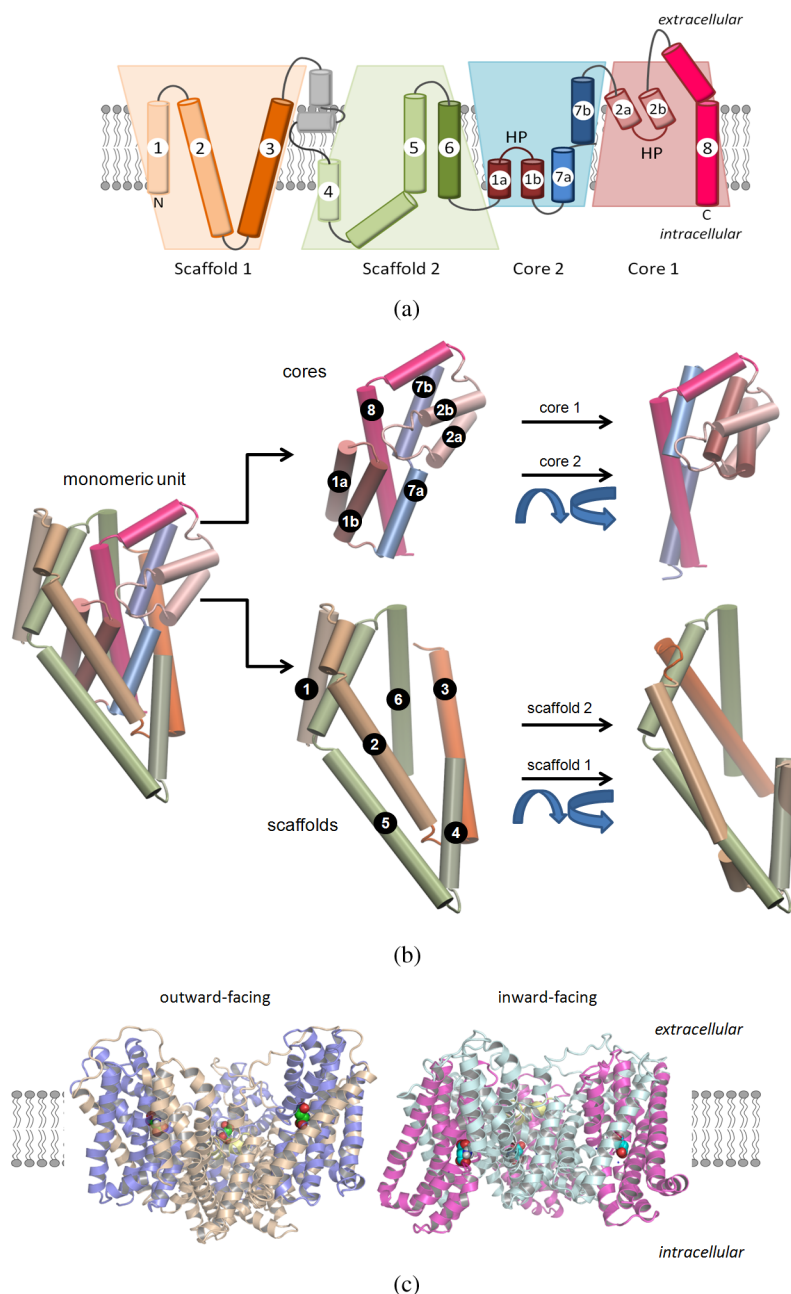


Figure 11. Generation of Glt_{ph} structure in the inward-facing state, by homology modeling based on outward-facing structure and symmetry considerations. (a) Glt_{ph} subunits consist each of two domains: scaffold and core, which, in turn, contain two symmetry-related topological repeats. (b) The two repeats in either the scaffold or the core can be closely superimposed upon rotation of one of the repeats by 180 degrees twice. (c) Crystal structures of the outward- and inward-facing states of the Glt_{ph} trimer. Note the vertical shift in the position of the core domains (purple/magenta ribbons) with respect to the scaffold (gray/cyan) in each subunit. The Asp⁻ in each subunit (CPK spheres) shifts from an EC-exposed state to an IC-exposed state upon the translation of the binding pocket rigidly embedded in the core domain.

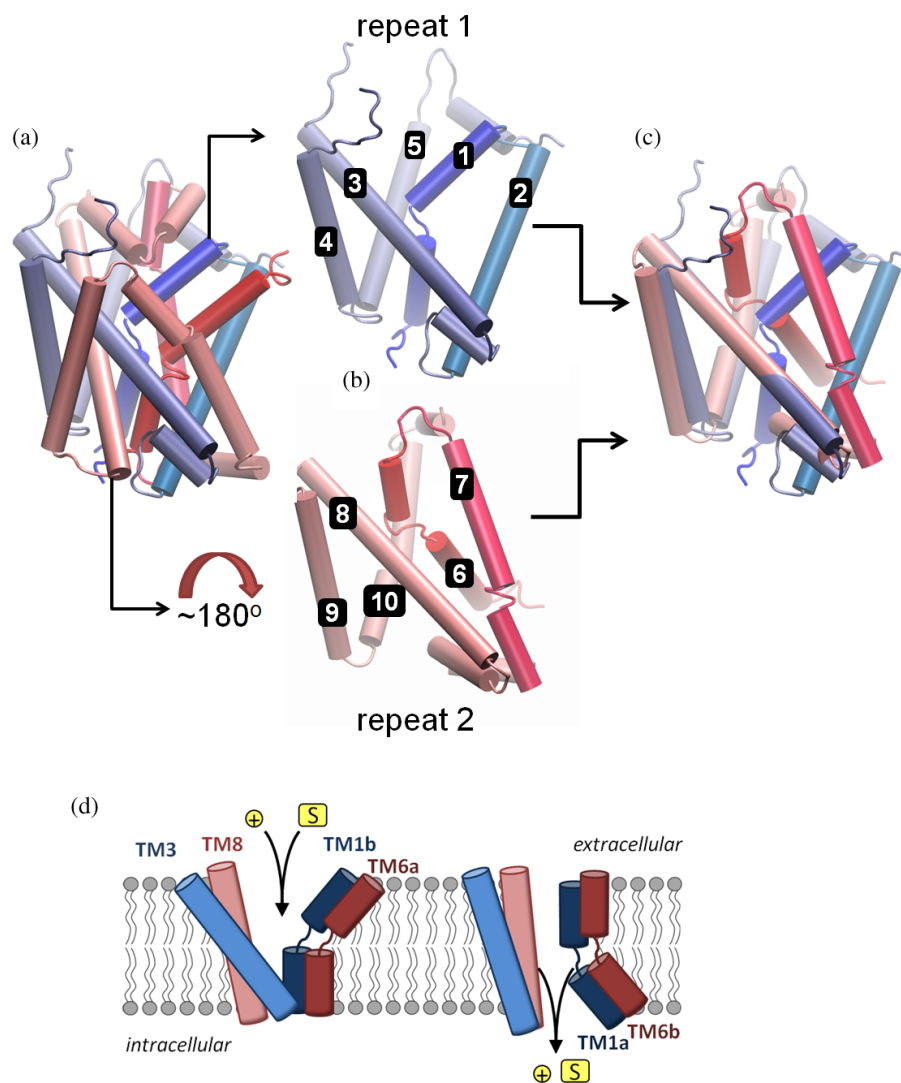


Figure 12. Homology modeling of the structure of NSS family members in the inward-facing state. (a–c) Pseudosymmetric organization of the first (blueish) and second (reddish) LeuT repeats. In this case, the first repeat is taken as is whereas the second is rotated by ~ 180 degrees (b) and aligned onto the first by superposition of TM3–5 and TM7–10 (c). Panel D gives a schematic description of the most prominent differences between the outward-facing crystal structure of LeuT (left) and the inward-facing crystal structure of vSGLT (right). TM helices are numbered according to LeuT.

Given that the inward-facing form of Mhp1 has been resolved only recently,⁶⁴ the structure of vSGLT in the inward-facing state, occluded form²⁸ served as a prototype for modeling the inward-facing conformation of NSS family members. In particular, a homology model for the inward-facing conformation of the eukaryotic serotonin transporter has been generated and experimentally validated.⁶³ Figure 12 summarizes the procedure for generating the inward-facing structural model for LeuT. As mentioned above, LeuT consists of two symmetrically related

structural repeats: TM1-TM5 and TM6-TM10. The last three helices in each repeat may be superimposed onto each other as illustrated in Figure 12a–12c. In LeuT, the first two helices of each repeat, (TM1 and TM2) and (TM6 and TM7), contain the substrate binding site and form the transport machinery. They are referred to as the “bundle”; whereas the last three helices of each repeat are referred to as the “scaffold”.⁶³ In the inward-facing model, the EC end of the bundle is closer to that of TM3 and TM8 (Figure 12d), whereas at the cytoplasmic side, the bundle is away from these two helices, exposing the substrate to the cytoplasm by opening an aqueous pathway from the binding site to the cytoplasm.⁶³ The generated model for the inward-facing state closely matches the crystal structure of vSGLT determined in the inward-facing state (Figure 11d).

5.2 Results from elastic network models

Although detailed all-atom simulations are an excellent source of information on local protein motions (e.g. the conformational changes along the horizontal arrows/steps in Figure 2), these methods have their limits. Global motions, such as the deformation between the inward- and outward-facing conformations, can alter a protein’s structure by several Ångstroms RMSD and take microseconds or longer time scales to complete. Exploring these motions in large molecules like sodium-coupled transporters requires the use of coarse-grained models that use simplifying approximations to reduce the molecule’s complexity. One such coarse-grained model that has been applied extensively to study the collective motions of biomolecular systems is the ENM. Computational analyses based on ENMs have proven in recent applications to shed light into conformational mechanisms relevant to the function (e.g. substrate binding, gating, etc.) of membrane proteins.⁶⁵

In a typical ENM, each amino acid is represented by a single point particle, or “node”, that is generally coincident with its C^α atom. Nodes within a certain interaction range (cutoff distance of about 7 Å or longer, depending on the particular ENM) are connected with springs, or “edges”, each of which has a resting length equal to the equilibrium distance between the nodes it joins. The potential energy of the resulting network is a sum over pairwise harmonic potentials with uniform spring constants, and represented by a single well centered about the native state in the multidimensional description of the energy landscape. The equilibrium dynamics can be decomposed into a set of normal modes of oscillation under this potential, each mode representative of a collective direction of reconfiguration or a basis vector that spans conformational space. Global motions can be estimated from the lowest frequency (or softest) modes.

Normal modes are commonly utilized for generating alternative structures of a protein to be used in predicting its substrate/inhibitor-bound forms, in studying its transitions between different functional forms, and in fitting high-resolution structures into lower-resolution experimental data such as the density maps from cryo-electron microscopy. The growing size of the PDB enables benchmarking ENMs and understanding its limitations. Recent analysis of large ensembles of soluble protein structures showed that, in general regardless of the size of the protein, the experimentally observed variations in NMR models closely relate to different functional forms determined by X-ray crystallography,⁶⁶ and these functional forms in turn conform to the intrinsic global dynamics of the proteins as predicted by ENM-NMA.^{67,68}

Here, we evaluate the ability of ENMs to predict the conformational transition from the outward-facing conformations of sodium-coupled transporters to inward-facing ones, or vice versa. Global modes of motion are calculated using the Anisotropic Network Model (ANM) with the standard cutoff distance of 15 Å.^{69,70} We compare the low-frequency spectrum of ANM modes to the deformation vectors inferred from experiments for (i) Glt_{ph} outward-to-inward transition (using the coordinates of the 1215 commonly resolved residues) and (ii) Mhp1 outward-to-inward transition (using 463 commonly resolved residues). As a metric of the correlation between predictions and experiments, we examine the level of cumulative overlap $(\sum_k \cos^2(\mathbf{d}, \mathbf{u}_k))^{1/2}$ between the structural change \mathbf{d} inferred from experiments (upon suitable superposition of known structures), and the modal changes (eigenvectors, \mathbf{u}_k) predicted by the ANM. Here suitable superposition means the elimination of the difference in six external degrees of freedom using Kabsch algorithm.⁷¹

Results are presented in Figure 13. The labels refer to the “starting structure” in each case, for which ANM calculations have been performed. As seen in panel A, the first 80 modes (or 2% of the complete set of ANM modes) can satisfactorily account for about 80% of the structural change between the inward-facing and outward-facing forms of Glt_{ph}. In the case of Mhp1, 30 modes (or 2%) account for about 60–70% of the change in the structure. These numbers are slightly lower than those obtained in studies of soluble globular proteins, for which around 80% correspondence is achieved by using 1–10 softest (non-degenerate) modes. Yet, they support

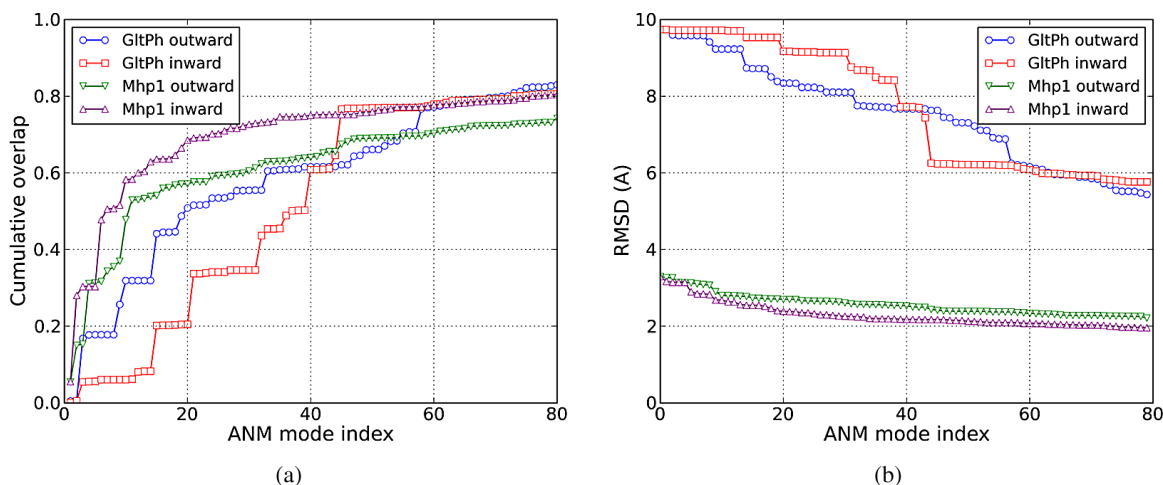


Figure 13. Examination of global transitions between the outward-facing and inward-facing structures of transporters using the ANM. (a) Cumulative overlap between the ANM modes of motion predicted for the indicated structures (see labels) and the experimentally observed structural changes between the alternative states of Glt_{ph} and Mhp1. The structural changes from experiments are described in terms of 3N-dimensional deformation vectors \mathbf{d} , which are compared with the 3N-dimensional eigenvectors predicted by the ANM. The deformation vector for Glt_{ph} is evaluated from the comparison of the PDB entries 1xfh and 3kbc for the respective outward- and inward-facing states. That of Mhp1 is evaluated using the PDB entries 1jln and 2x79. (b) Gradual reconfiguration of a given structure (labeled) during stepwise movements along the ANM soft modes. The RMSDs between the instantaneous conformations and the target structures are shown.

the view that a small subset of modes in the lowest frequency end of the mode spectrum can be advantageously exploited for exploring the conformational subspace where the functional transitions take place.

We also note the stepwise increases in cumulative overlap at particular modes of Glt_{ph} . Consistent with earlier studies, these are non-degenerate modes: they induce three-fold symmetric changes, equally affecting all three subunits. For example, the outward-facing state of Glt_{ph} favors a global opening/closing of the aqueous basin (mode 3), which alone contributes by ~ 0.2 to the cumulative overlap between predictions and experiments.⁶⁵ A similar feature is observed for the second ANM mode accessible to the Mhp1 , suggesting that this mode plays a significant role in establishing the transition from the inward-facing state of Mhp1 to its outward-facing state.

In addition, the RMSD between the ANM-predicted instantaneous conformation and the target structure may be probed, as the starting conformation gradually reconfigures along the soft modes. Figure 13b displays the decrease in RMSD obtained for the two test cases' forward and reverse transitions. For Glt_{ph} , the movement in the subspace of 70 ANM modes decreases the RMSD from 9.75 Å to about 5.5 Å upon starting from either conformation. For Mhp1 , the decrease in RMSD is from 3.3 Å to 2 Å. These results suggest that the ANM can partially account for the structural changes observed in sodium-coupled transporters, and a few soft modes (about 2%) provide a reasonable estimate of the initial steps along the transition pathway. Further improvement in the methodology (and agreement with experiments) may presumably be achieved (i) upon more accurate description of the potentials (e.g. force constants) between interacting pair of residues to account for chain connectivity or other sequence-specific effects, and/or (ii) by explicitly taking the effect of the lipid bilayer into consideration in the analysis. The growing number of membrane protein structures will certainly guide us in developing more suitable ENMs or other coarse-grained models and methods.

6. Conclusion

Knowledge of transporter structure is a significant step towards gaining insights into the critical interactions that mediate substrate binding and translocation, or the structural determinants of the particular biological function. Structural data become especially useful when multiple structures along the translocation cycle are resolved. But, the information deduced from these structures on the molecular mechanisms of substrate transfer is only indirect: the detailed mechanisms and time evolution of the role of Na^+ ions or the conformational changes that control substrate translocation cannot be inferred from static structures. The resolved structures are, as we have shown, snapshots of a continuum of processes. Simulations conducted with resolved structures reveal the detailed (atomic scale) mechanisms of gate opening and closing events and substrate/cation release. Likewise, the "occluded" vSGLT conformer has been revealed by simulations to readily provide access to Na^+ migration to the cytoplasm. Simulations with Glt_{ph} outward-facing structure also revealed the role of Na^+ ions in stabilizing the closed form of the EC gate after substrate binding. Finally, coarse-grained simulations provide insights into evolutionarily optimized patterns/mechanisms that enable the transition between inward-facing and outward-facing states of these transporters. The pathway of transition between alternative functional states may now be efficiently explored by taking steps in the subspace spanned by soft modes. While there are significant

advances in single-molecule measurements and detection of time-resolved data or transition events, for the most part, the collection of such data at atomic resolution is very hard, if not impossible. Likewise, while a number of structures along the allosteric cycle are known, a complete description of the sequence of events and their driving mechanisms at the microscopic scale is still lacking. Structure-based computations serve as important tools for improving our understanding of the molecular mechanisms of biological function, and are expected to become even more useful in the future with increasing data on the membrane proteins structures and function that will allow for optimizing computational models and methods.

References

1. C. J. Law, P. C. Maloney and D. N. Wang. 2008. Ins and outs of major facilitator superfamily antiporters. *Annu Rev Microbiol* **62**, 289–305.
2. B. Poolman. 1990. Precursor/product antiport in bacteria. *Mol Microbiol* **4**, 1629–1636.
3. B. I. Kanner and E. Zomot. 2008. Sodium-coupled neurotransmitter transporters. *Chem Rev* **108**, 1654–1668.
4. G. E. Torres and S. G. Amara. 2007. Glutamate and monoamine transporters: New visions of form and function. *Curr Opin Neurobiol* **17**, 304–312.
5. C. I. Wang and R. J. Lewis. 2010. Emerging structure-function relationships defining monoamine NSS transporter substrate and ligand affinity. *Biochem Pharmacol* **79**, 1083–1091.
6. T. S. Ikeda, E. S. Hwang, M. J. Coady, B. A. Hirayama, M. A. Hediger and E. M. Wright. 1989. Characterization of a Na⁺/glucose cotransporter cloned from rabbit small intestine. *J Membr Biol* **110**, 87–95.
7. E. Padan, M. Venturi, Y. Gerchman and N. Dover. 2001. Na⁺/H⁺ antiporters. *Biochim Biophys Acta* **1505**, 144–157.
8. J. Orłowski and S. Grinstein. 2004. Diversity of the mammalian sodium/proton exchanger SLC9 gene family. *Pflugers Arch* **447**, 549–565.
9. J. M. Wood. 2007. Bacterial osmosensing transporters. *Methods Enzymol* **428**, 77–107.
10. S. Ressler, A. C. Terwisscha van Scheltinga, C. Vornrhein, V. Ott and C. Ziegler. 2009. Molecular basis of transport and regulation in the Na⁺/betaine symporter BetP. *Nature* **458**, 47–52.
11. K. Tanaka, K. Watase, T. Manabe, K. Yamada, M. Watanabe, K. Takahashi, H. Iwama, T. Nishikawa, N. Ichihara, T. Kikuchi, S. Okuyama, N. Kawashima, S. Hori, M. Takimoto and K. Wada. 1997. Epilepsy and exacerbation of brain injury in mice lacking the glutamate transporter GLT-1. *Science* **276**, 1699–1702.
12. N. Zerangue and M. P. Kavanaugh. 1996. Flux coupling in a neuronal glutamate transporter. *Nature* **383**, 634–637.
13. S. G. Amara and A. C. Fontana. 2002. Excitatory amino acid transporters: Keeping up with glutamate. *Neurochem Int* **41**, 313–318.
14. N. C. Danbolt. 2001. Glutamate uptake. *Prog Neurobiol* **65**, 1–105.
15. B. I. Kanner. 1994. Sodium-coupled neurotransmitter transport: Structure, function and regulation. *J Exp Biol* **196**, 237–249.
16. A. L. Lomize, I. D. Pogozheva, M. A. Lomize and H. I. Mosberg. 2006. Positioning of proteins in membranes: A computational approach. *Protein Sci* **15**, 1318–1333.

17. M. H. Saier, Jr. and Q. Ren. 2006. The bioinformatic study of transmembrane molecular transport. *J Mol Microbiol Biotechnol* **11**, 289–290.
18. O. Boudker, R. M. Ryan, D. Yernool, K. Shimamoto and E. Gouaux. 2007. Coupling substrate and ion binding to extracellular gate of a sodium-dependent aspartate transporter. *Nature* **445**, 387–393.
19. N. Reyes, C. Ginter and O. Boudker. 2009. Transport mechanism of a bacterial homologue of glutamate transporters. *Nature* **462**, 880–885.
20. D. Yernool, O. Boudker, Y. Jin and E. Gouaux. 2004. Structure of a glutamate transporter homologue from *Pyrococcus horikoshii*. *Nature* **431**, 811–818.
21. A. Yamashita, S. K. Singh, T. Kawate, Y. Jin and E. Gouaux. 2005. Crystal structure of a bacterial homologue of Na⁺/Cl⁻ dependent neurotransmitter transporters. *Nature* **437**, 215–223.
22. T. L. Whitworth, L. C. Herndon and M. W. Quick. 2002. Psychostimulants differentially regulate serotonin transporter expression in thalamocortical neurons. *J Neurosci* **22**, RC192.
23. T. Beuming, J. Kniazeff, M. L. Bergmann, L. Shi, L. Gracia, K. Raniszewska, A. H. Newman, J. A. Javitch, H. Weinstein, U. Gether and C. J. Loland. 2008. The binding sites for cocaine and dopamine in the dopamine transporter overlap. *Nat Neurosci* **11**, 780–789.
24. E. M. Wright, D. D. Loo, B. A. Hirayama and E. Turk. 2004. Surprising versatility of Na⁺-glucose cotransporters: SLC5. *Physiology (Bethesda)* **19**, 370–376.
25. E. M. Wright, B. A. Hirayama and D. F. Loo. 2007. Active sugar transport in health and disease. *J Intern Med* **261**, 32–43.
26. J. Francis, J. Zhang, A. Farhi, H. Carey and D. S. Geller. 2004. A novel SGLT2 mutation in a patient with autosomal recessive renal glucosuria. *Nephrol Dial Transplant* **19**, 2893–2895.
27. E. M. Wright, E. Turk and M. G. Martin. 2002. Molecular basis for glucose-galactose malabsorption. *Cell Biochem Biophys* **36**, 115–121.
28. S. Faham, A. Watanabe, G. M. Besserer, D. Cascio, A. Specht, B. A. Hirayama, E. M. Wright and J. Abramson. 2008. The crystal structure of a sodium galactose transporter reveals mechanistic insights into Na⁺/sugar symport. *Science* **321**, 810–814.
29. J. Li and E. Tajkhorshid. 2009. Ion-releasing state of a secondary membrane transporter. *Biophys J* **97**, L29–L31.
30. E. Zomot and I. Bahar. 2010. The sodium/galactose symporter crystal structure is a dynamic, not so occluded state. *Mol Biosyst* **6**, 1040–1046.
31. P. Mitchell. 1957. A general theory of membrane transport from studies of bacteria. *Nature* **180**, 134–136.
32. I. Smirnova, V. Kasho, J. Sugihara and H. R. Kaback. 2009. Probing of the rates of alternating access in LacY with Trp fluorescence. *Proc Natl Acad Sci U S A* **106**, 21561–21566.
33. I. Smirnova, V. Kasho, J. Y. Choe, C. Altenbach, W. L. Hubbell and H. R. Kaback. 2007. Sugar binding induces an outward facing conformation of LacY. *Proc Natl Acad Sci U S A* **104**, 16504–16509.
34. L. Guan and H. R. Kaback. 2006. Lessons from lactose permease. *Annu Rev Biophys Biomol Struct* **35**, 67–91.
35. L. R. Forrest, S. Tavoulari, Y. W. Zhang, G. Rudnick and B. Honig. 2007. Identification of a chloride ion binding site in Na⁺/Cl⁻-dependent transporters. *Proc Natl Acad Sci U S A* **104**, 12761–12766.
36. E. Zomot, A. Bendahan, M. Quick, Y. Zhao, J. A. Javitch and B. I. Kanner. 2007. Mechanism of chloride interaction with neurotransmitter:sodium symporters. *Nature* **449**, 726–730.
37. S. K. Singh, A. Yamashita and E. Gouaux. 2007. Antidepressant binding site in a bacterial homologue of neurotransmitter transporters. *Nature* **448**, 952–956.

38. S. K. Singh, C. L. Piscitelli, A. Yamashita and E. Gouaux. 2008. A competitive inhibitor traps LeuT in an open-to-out conformation. *Science* **322**, 1655–1661.
39. L. Tang, L. Bai, W. H. Wang and T. Jiang. 2010. Crystal structure of the carnitine transporter and insights into the antiport mechanism. *Nat Struct Mol Biol* **17**, 492–496.
40. S. Weyand, T. Shimamura, S. Yajima, S. Suzuki, O. Mirza, K. Krusong, E. P. Carpenter, N. G. Rutherford, J. M. Hadden, J. O'Reilly, P. Ma, M. Saidijam, S. G. Patching, R. J. Hope, H. T. Norbertczak, P. C. Roach, S. Iwata, P. J. Henderson and A. D. Cameron. 2008. Structure and molecular mechanism of a nucleobase-cation-symport-1 family transporter. *Science* **322**, 709–713.
41. W. Humphrey, A. Dalke and K. Schulten. 1996. VMD: Visual molecular dynamics. *J Mol Graph* **14**, 33–38.
42. E. Gouaux. 2009. Review. The molecular logic of sodium-coupled neurotransmitter transporters. *Philos Trans R Soc Lond B Biol Sci* **364**, 149–154.
43. H. Krishnamurthy, C. L. Piscitelli and E. Gouaux. 2009. Unlocking the molecular secrets of sodium-coupled transporters. *Nature* **459**, 347–355.
44. D. A. Caplan, J. O. Subbotina and S. Y. Noskov. 2008. Molecular mechanism of ion-ion and ion-substrate coupling in the Na⁺-dependent leucine transporter LeuT. *Biophys J* **95**, 4613–4621.
45. S. Y. Noskov and B. Roux. 2008. Control of ion selectivity in LeuT: Two Na⁺ binding sites with two different mechanisms. *J Mol Biol* **377**, 804–818.
46. I. Bahar, T. R. Lezon, L. W. Yang and E. Eyal. 2010. Global dynamics of proteins: bridging between structure and function. *Annu Rev Biophys* **39**, 23–42.
47. I. H. Shrivastava, J. Jiang, S. G. Amara and I. Bahar. 2008. Time-resolved mechanism of extracellular gate opening and substrate binding in a glutamate transporter. *J Biol Chem* **283**, 28680–28690.
48. Z. Huang and E. Tajkhorshid. 2008. Dynamics of the extracellular gate and ion-substrate coupling in the glutamate transporter. *Biophys J* **95**, 2292–2300.
49. J. Dechancie and I. Bahar. 2011. The mechanism of substrate release by the aspartate transporter Glt(Ph): Insights from simulations. *Mol Biosyst* **7**, 832–842.
50. X. Gao, L. Zhou, X. Jiao, F. Lu, C. Yan, X. Zeng, J. Wang and Y. Shi. 2010. Mechanism of substrate recognition and transport by an amino acid antiporter. *Nature* **463**, 828–832.
51. S. Y. Noskov and B. Roux. 2008. Control of ion selectivity in LeuT: Two Na⁺ binding sites with two different mechanisms. *J Mol Biol* **377**, 804–818.
52. D. A. Caplan, J. O. Subbotina and S. Y. Noskov. 2008. Molecular mechanism of ion-ion and ion-substrate coupling in the Na⁺-dependent leucine transporter *LeuT* *Biophys J* **95**, 4613–4621.
53. T. Wein and K. T. Wanner. 2009. Generation of a 3D model for human GABA transporter hGAT-1 using molecular modeling and investigation of the binding of GABA. *J Mol Model* **16**, 155–161.
54. X. Huang and C. G. Zhan. 2007. How dopamine transporter interacts with dopamine: Insights from molecular modeling and simulation. *Biophys J* **93**, 3627–3639.
55. P. C. Gedeon, M. Indarte, C. K. Surratt and J. D. Madura. 2010. Molecular dynamics of leucine and dopamine transporter proteins in a model cell membrane lipid bilayer. *Proteins* **78**, 797–811.
56. L. Celik, B. Schiott and E. Tajkhorshid. 2008. Substrate binding and formation of an occluded state in the leucine transporter. *Biophys J* **94**, 1600–1612.
57. Y. Gu, I. H. Shrivastava, S. G. Amara and I. Bahar. 2009. Molecular simulations elucidate the substrate translocation pathway in a glutamate transporter. *Proc Natl Acad Sci U S A* **106**, 2589–2594.

58. L. Shi, M. Quick, Y. Zhao, H. Weinstein and J. A. Javitch. 2008. The mechanism of a neurotransmitter:sodium symporter — inward release of Na⁺ and substrate is triggered by substrate in a second binding site. *Mol. Cell* **30**, 667–677.
59. Z. Zhou, J. Zhen, N. K. Karpowich, R. M. Goetz, C. J. Law, M. E. Reith and D. N. Wang. 2007. LeuT-desipramine structure reveals how antidepressants block neurotransmitter reuptake. *Science* **317**, 1390–1393.
60. M. Quick, A. M. Winther, L. Shi, P. Nissen, H. Weinstein and J. A. Javitch. 2009. Binding of an octylglucoside detergent molecule in the second substrate (S2) site of LeuT establishes an inhibitor-bound conformation. *Proc Natl Acad Sci U S A* **106**, 5563–5568.
61. E. Turk, O. Kim, C. J. Je, J. P. Whitelegge, S. Eskandari, J. T. Lam, M. Kreman, G. Zampighi, K. F. Faull and E. M. Wright. 2000. Molecular characterization of *Vibrio parahaemolyticus* vSGLT: A model for sodium-coupled sugar cotransporters. *J Biol Chem* **275**, 25711–25716.
62. T. J. Crisman, S. Qu, B. I. Kanner and L. R. Forrest. 2009. Inward-facing conformation of glutamate transporters as revealed by their inverted-topology structural repeats. *Proc Natl Acad Sci U S A* **106**, 20752–20757.
63. L. R. Forrest, Y. W. Zhang, M. T. Jacobs, J. Gesmonde, L. Xie, B. H. Honig and G. Rudnick. 2008. Mechanism for alternating access in neurotransmitter transporters. *Proc Natl Acad Sci U S A* **105**, 10338–10343.
64. T. Shimamura, S. Weyand, O. Beckstein, N. G. Rutherford, J. M. Hadden, D. Sharples, M. S. Sansom, S. Iwata, P. J. Henderson and A. D. Cameron. 2010. Molecular basis of alternating access membrane transport by the sodium-hydantoin transporter Mhp1. *Science* **328**, 470–473.
65. I. Bahar, T. R. Lezon, A. Bakan and I. H. Shrivastava. 2010. Normal mode analysis of biomolecular structures: functional mechanisms of membrane proteins. *Chem Rev* **110**, 1463–1497.
66. O. F. Lange, N. A. Lakomek, C. Fares, G. F. Schroder, K. F. Walter, S. Becker, J. Meiler, H. Grubmüller, C. Griesinger and B. L. de Groot. 2008. Recognition dynamics up to microseconds revealed from an RDC-derived ubiquitin ensemble in solution. *Science* **320**, 1471–1475.
67. A. Bakan and I. Bahar. 2009. The intrinsic dynamics of enzymes plays a dominant role in determining the structural changes induced upon inhibitor binding. *Proc Natl Acad Sci U S A* **106**, 14349–14354.
68. L. Yang, G. Song, A. Carriquiry and R. L. Jernigan. 2008. Close correspondence between the motions from principal component analysis of multiple HIV-1 protease structures and elastic network modes. *Structure* **16**, 321–330.
69. A. R. Atilgan, S. R. Durell, R. L. Jernigan, M. C. Demirel, O. Keskin and I. Bahar. 2001. Anisotropy of fluctuation dynamics of proteins with an elastic network model. *Biophys J* **80**, 505–515.
70. E. Eyal, L. W. Yang and I. Bahar. 2006. Anisotropic network model: Systematic evaluation and a new web interface. *Bioinformatics* **22**, 2619–2627.
71. W. Kabsch. 1976. A solution for the best rotation to relate two sets of vectors. *Acta Crystallographica Section A* **32**, 922–923.

